doi:10.1093/brain/aws262 Brain 2013: 136; 147–167 | 147

BRAIN
A JOURNAL OF NEUROLOGY

Astrocytes regulate myelin clearance through recruitment of microglia during cuprizone-induced demyelination

Thomas Skripuletz,[1,*] Diane Hackstette,[1,*] Katharina Bauer,[1] Viktoria Gudi,[1] Refik Pul,[1] Elke Voss,[1] Katharina Berger,[2] Markus Kipp,[2] Wolfgang Baumgärtner[3,4] and Martin Stangel[1,4]

1 Department of Neurology, Hannover Medical School, Hannover, Germany
2 Institute of Neuroanatomy, Faculty of Medicine, RWTH Aachen University, Aachen, Germany
3 Department of Pathology, University of Veterinary Medicine Hannover, Hannover, Germany
4 Center for Systems Neuroscience, Hannover, Germany

*These authors contributed equally to this work.

Correspondence to: Professor Dr Martin Stangel,
Department of Neurology,
Hannover Medical School,
Carl-Neuberg-Str-1,
30625 Hannover,
Germany
E-mail: Stangel.Martin@MH-Hannover.de

Recent evidence suggests that astrocytes play an important role in regulating de- and remyelination in multiple sclerosis. The role of astrocytes is controversial, and both beneficial as well as detrimental effects are being discussed. We performed loss-of-function studies based on astrocyte depletion in a cuprizone-induced rodent model of demyelination. This led to strong astrogliosis accompanied by microgliosis and demyelination in C57BL/6 wild-type mice. Ablation of astrocytes in glial fibrillary acidic protein–thymidine kinase transgenic mice was associated with a failure of damaged myelin removal and a consecutive delay in remyelination. Despite oligodendrocyte death, myelin was still present, but ultrastructual investigations showed that the myelin structure was loosened and this damaged myelin did not protect axons. These alterations were associated with a decrease in microglial activation. Thus, our results show that astrocyte loss does not prevent myelin damage, but clearance of damaged myelin through recruitment of microglia is impaired. Further studies suggest that this process is regulated by the chemokine CXCL10. As a consequence of the delayed removal of myelin debris, remyelination and oligodendrocyte precursor cell proliferation were impaired. Experiments omitting the influence of myelin debris demonstrated an additional beneficial effect of astrocytes on oligodendrocyte regeneration during remyelination. In conclusion, these data demonstrate for the first time *in vivo* that astrocytes provide the signal environment that forms the basis for the recruitment of microglia to clear myelin debris, a process required for subsequent repair mechanisms. This is of great importance to understanding regenerative processes in demyelinating diseases such as multiple sclerosis.

Keywords: astrocytes; cuprizone; demyelination; microglia; myelin

Abbreviations: APC = anti-adenomatus polyposis coli; APP = amyloid precursor protein; CNPase = cyclic nucleotide 3′-phosphodiesterase; EAE = experimental autoimmune encephalomyelitis; GFAP = glial fibrillary acidic protein; Iba-1 = ionized calcium-binding adaptor molecule 1; RCA-1 = lectin *ricinus communis* agglutinin 1

Received March 29, 2012. Revised July 16, 2012. Accepted August 5, 2012. Advance Access publication December 24, 2012

Introduction

Multiple sclerosis is a chronic inflammatory disease of the CNS that leads to demyelination of white and grey matter (Kieseier and Stuve, 2011; Stadelmann *et al*., 2011). Remyelination is the natural regenerative mechanism of demyelination, and it is proposed that remyelinated axons are protected from degeneration (Franklin and Kotter, 2008). Unfortunately remyelination is highly variable in patients with multiple sclerosis, and for reasons not well understood, remyelination often fails or is incomplete.

Although new aspects of underlying pathomechanisms leading to de- and remyelination are being discovered continuously, the complex biological interactions are far from being completely understood. Recent evidence suggests that astrocytes may play a key role in regulating demyelinating CNS diseases (Nair *et al*., 2008). Reactive astrocytosis is a prominent feature in inflammatory CNS conditions that occur in multiple sclerosis and experimental autoimmune encephalomyelitis (EAE), an inflammation-driven animal model of CNS demyelination (Eng and Ghirnikar, 1994; Bannerman *et al*., 2007; Guo *et al*., 2011). Apart from the typical morphology with star-like projections, astrocytes are distinguished by their expression of the intermediate glial fibrillary acidic protein (GFAP). On activation, astrocytes upregulate the expression of GFAP in a process called gliosis (Eng, 1985).

The role of astrocytes in demyelinating diseases is controversial, and both protective as well as deleterious effects on demyelination are being discussed (Williams *et al*., 2007; De Keyser *et al*., 2010; Moore *et al*., 2011). Astrocytes are suggested to exert detrimental effects and promote demyelination by enhancing the immune response through expression of cytokines and recruitment of T cells, microglia and macrophages to demyelinating lesions. As astrocytes are the main producers of chemokines in multiple sclerosis, it was suggested that chemokine secretion may be the primary way in which astrocytes perpetuate immune-mediated demyelination.

In contrast, favourable effects of astrocytes on demyelination have also been proposed. The formation of a glial scar is supposed to be a physical barrier against inflammatory cells entering demyelinated areas (Nair *et al*., 2008). Accordingly, in transgenic mice, ablation of proliferating astrocytes in EAE disrupts the formation of the glial scar and is associated with increased recruitment of inflammatory cells, including T cells, neutrophils and macrophages, into the CNS (Voskuhl *et al*., 2009). In consequence, the exacerbated inflammation is associated with a more severe and rapidly fulminant clinical course of EAE. Astrocytes may also attenuate the inflammatory response through the production of anti-inflammatory cytokines, such as interleukin 10, transforming growth factor-β and interleukin 27 (Nair *et al*., 2008).

Because many of these studies were performed under *in vitro* conditions, our experiments aimed to give new insights into the role of astrocytes in an *in vivo* model of experimental demyelination. We performed detailed loss-of-function studies based on astrocyte depletion and used a well-characterized rodent model of cuprizone-induced demyelination. This rather robust model allows analysis of demyelination in the white and grey matter of the CNS, which is accompanied by a strong astrogliosis, without the interference of the peripheral immune system (Matsushima and Morell, 2001; Kipp *et al*., 2009; Skripuletz *et al*., 2011*a*).

Materials and methods

Animals

To ablate reactive astrocytes selectively, GFAP–thymidine kinase transgenic mouse line 7.1 (The Jackson Laboratory) was used, in which thymidine kinase from the herpes simplex virus is targeted to astrocytes using the mouse GFAP promoter (Bush *et al*., 1998). GFAP–thymidine kinase transgenic mice were obtained by mating heterozygous female mice of GFAP–thymidine kinase line 7.1 with wild-type C57BL/6 male mice. GFAP–thymidine kinase mice develop normally, exhibit no changes of brain structure and are indistinguishable from wild-type littermates (Myer *et al*., 2006).

Mice were genotyped by PCR for herpes simplex virus thymidine kinase. Animals underwent routine cage maintenance once a week and were microbiologically monitored according to the Federation of European Laboratory Animal Science Association's recommendations (Rehbinder *et al*., 1996). Food and water were available *ad libitum*. All research and animal care procedures were approved by the review board for the care of animal subjects of the district government (Lower Saxony, Germany) and performed according to international guidelines on the use of laboratory animals.

Treatment of GFAP–thymidine kinase mice with ganciclovir selectively and specifically ablates astrocytes expressing GFAP–thymidine kinase through a non-inflammatory apoptotic mechanism both *in vivo* and *in vitro* (Bush *et al*., 1998, 1999). Ganciclovir is a nucleoside analogue that is phosphorylated by herpes simplex virus thymidine kinase within GFAP-positive cells. Phosphorylated ganciclovir competes with endogenous nucleotide triphosphates and disrupts DNA synthesis, thereby triggering apoptotic cell death of proliferating cells. The efficacy and specificity of this ablation of proliferating astrocytes have been shown and confirmed in a number of studies (Bush *et al*., 1999; Faulkner *et al*., 2004; Voskuhl *et al*., 2009).

Induction of experimental demyelination

Experimental demyelination was induced by feeding 8-week-old male GFAP–thymidine kinase transgenic mice and wild-type C57BL/6 mice a diet containing 0.2% cuprizone (bis-cyclohexanone oxaldihydrazone, Sigma-Aldrich) mixed into a ground standard rodent chow (Skripuletz *et al*., 2011*a*). The cuprizone diet was maintained for 5 weeks.

To investigate the effect of astrocyte ablation on demyelination, cuprizone-fed GFAP–thymidine kinase transgenic mice were treated with ganciclovir (25 mg/kg in 200 µl of PBS) intraperitoneally every day, beginning on the day of cuprizone feeding until termination of the experiment (for experimental design, see Supplementary Fig. 1A). This ganciclovir injection protocol was identified as sufficient to cause ablation of 60–70% of astrocytes in transgenic mice. Control GFAP–thymidine kinase transgenic mice were fed with cuprizone and were injected with PBS only. Control wild-type C57BL/6 mice were fed with cuprizone and were treated intraperitoneally with ganciclovir or PBS. Additional control models included GFAP–thymidine kinase transgenic mice fed with normal chow and injected with ganciclovir or PBS and C57BL/6 mice injected with PBS.

At different time points (3, 4 and 5 weeks), mice were perfused with 4% paraformaldehyde in phosphate buffer through the left cardiac

ventricle as previously described (Gudi *et al*., 2009). The brains were removed, postfixed in 4% paraformaldehyde and paraffin embedded. For light microscopy, 7-μm serial paraffin sections were cut and dried at 37°C overnight. Sections between bregma −0.82 mm and bregma −1.82 mm according to the mouse atlas by Paxinos and Franklin (2001) were analysed.

For PCR analysis, mice were perfused with ice-cold PBS through the left cardiac ventricle to clear blood cells from the intravascular compartment. The brains were removed and stored in ice-cold Hanks' balanced salt solution (Sigma-Aldrich) containing 15 mM N-2-Hydroxyethylpiperazine-N′-2-ethanesulfonic acid (HEPES) buffer and 5% glucose. Corpus callosum and cerebral cortex were dissected from whole brains under a light microscope.

For immunohistochemistry, a group of six animals was investigated at all time points, whereas three animals were investigated for PCR or electron microscopic analyses, respectively.

To investigate further the effect of late astrocyte ablation on demyelination, two different injection protocols were used (for experimental design, see Supplementary Fig. 1B). In one experimental setting, ganciclovir or PBS injections were started after Week 3 of cuprizone treatment (start of microglial infiltration and demyelination), whereas in the second experimental setting, injections were given after Week 4 (time of the peak of microglial infiltration and severe demyelination). Cuprizone-fed GFAP–thymidine kinase transgenic mice were injected with a higher dose of ganciclovir at first injection, with the aim of inducing sufficient loss of astrocytes [200 mg (in 200 μl of PBS) ganciclovir per kg]. Thereafter, ganciclovir was given every day until termination of the experiment at a dose of 25 mg (in 200 μl of PBS) of ganciclovir per kg as described earlier in the text. For each experimental setting, control GFAP–thymidine kinase transgenic mice were fed with cuprizone and were injected with PBS only. Control wild-type C57BL/6 mice were fed with cuprizone and were treated with ganciclovir or PBS as described earlier in the text. A group size of six animals was analysed at Week 5, the time point of complete demyelination of the corpus callosum. For immunohistochemistry, mice were perfused with 4% paraformaldehyde in phosphate buffer through the left cardiac ventricle, and brains were removed as described earlier.

To analyse the long-term effects of astrocyte ablation on demyelination, the cuprizone diet was maintained for 6 weeks. Cuprizone-fed GFAP–thymidine kinase transgenic mice received ganciclovir (25 mg/kg in 200 μl of PBS) intraperitoneally every day, beginning on the day of cuprizone feeding until termination of the experiment (for experimental design, see Supplementary Fig. 1C). The control groups included (i) GFAP–thymidine kinase transgenic mice fed with cuprizone and injected with PBS; (ii) wild-type C57BL/6 mice fed with cuprizone and injected with ganciclovir or PBS; (iii) GFAP–thymidine kinase transgenic mice fed with normal chow and injected with ganciclovir or PBS and (iv) C57BL/6 mice injected with PBS. For immunohistochemistry, a group size of six animals was investigated.

To investigate the effect of astrocyte ablation on remyelination, the cuprizone diet was withdrawn after 5 weeks, and mice were fed with normal food to allow remyelination (for experimental design, see Supplementary Fig. 1D). Ganciclovir or PBS injections were started after Week 4 of cuprizone treatment. At first injection, ganciclovir was given at a dose of 200 mg/kg in 200 μl of PBS. Thereafter, ganciclovir was given every day until termination of the experiment at a dose of 25 mg/kg in 200 μl of PBS. Control GFAP–thymidine kinase transgenic mice were fed with cuprizone and were injected with PBS, and control wild-type C57BL/6 mice were fed with cuprizone and were treated with ganciclovir or PBS, as described earlier in the text. A group size of six animals was analysed.

Histology, immunohistochemistry and electron microscopy

Histology and immunohistochemistry were performed as described previously (Gudi *et al*., 2009; Skripuletz *et al*., 2010*a*). See Supplementary material for details.

The following primary antibodies were used: for astrocytes, GFAP mouse immunoglobulin G1 (1:200, Millipore) or rabbit immunoglobulin G (1:200, DakoCytomation) and vimentin rabbit immunoglobulin G (1:500, Epitomics); for myelin proteolipid protein, mouse immunoglobulin G2a (1:500, Serotec), myelin-associated glycoprotein (mouse immunoglobulin G1, 1:1000, Abcam), myelin oligodendrocyte glycoprotein (1:2 hybridoma supernatant, gift from C. Linington), cyclic nucleotide 3′-phosphodiesterase (CNPase; 1:200, mouse immunoglobulin G, Millipore) and myelin basic protein (1:500, mouse immunoglobulin G, Covance); for microglia, the lectin *Ricinus communis* agglutinin 1 (RCA-1; biotinylated, 1:1000, Vector Laboratories), Mac-3 (rat immunoglobulin G1, 1:500, BD Pharmingen) and ionized calcium-binding adaptor molecule 1 (Iba-1; rabbit anti-Iba-1, 1:1000, Wako); for oligodendrocytes, Nogo-A (rabbit immunoglobulin G, 1:750, Millipore) and anti-adenomatus polyposis coli (APC; mouse immunoglobulin G2b, 1:200, Calbiochem); for oligodendrocyte precursor cells, Olig-2 (rabbit immunoglobulin G, 1:500, Millipore); for proliferation, Ki-67 (mouse immunoglobulin G1, 1:50, BD Pharmingen); for axonal damage, amyloid precursor protein (APP; mouse immunoglobulin G1, 1:800, Millipore) and synaptophysin (mouse immunoglobulin G1, 1:200, Serotec) and for the chemokine, CXCL10 (mouse immunoglobulin G, 1:100, Santa Cruz).

For electron microscopy, Epon embedding was performed as previously described (Lindner *et al*., 2008). See Supplementary material for details.

Quantification of glial reactions

Quantification of glial cells was performed for astrocytes (GFAP, vimentin), proliferating astrocytes (double staining for Ki-67/GFAP), mature oligodendrocytes (Nogo-A, APC) and activated microglia (RCA-1, Mac-3). Immunopositive cells and non–nucleus-associated APP and synaptophysin-positive axons in the corpus callosum were counted in the central part in an area of at least 0.185 mm^2 using a magnification of ×400. In the cerebral cortex, counting of immunopositive cells with identifiable nuclei [counterstaining with Mayer's haemalum solution for immunohistochemistry and 4′,6-diamidino-2-phenylindole (DAPI) for immunofluorescence] was performed for the cell layers 1-6 in both left and right hemispheres at least within an area of 1.125 mm^2 using a magnification of ×400 (Olympus BX61) as previously described (Gudi *et al*., 2009). Counted cells are expressed as number of cells/mm^2.

Determination of de- and remyelination

The extent of demyelination in the corpus callosum and cerebral cortex was analysed as described previously (Skripuletz *et al*., 2008, 2010*b*). For determination of demyelination in the corpus callosum, sections stained with Luxol fast blue, myelin proteolipid protein, myelin-associated glycoprotein and myelin oligodendrocyte glycoprotein were scored in a blinded manner by three observers and graded on a scale from 0 (complete demyelination) to 3 (normal myelin). In addition to white matter demyelination, the complete cortex was subsequently analysed by light microscopy (Olympus BX61), and myelin proteolipid protein- and myelin-associated glycoprotein-stained

sections were scored by three blinded observers using a scale from 0 (complete demyelination) to 4 (normal myelin) as previously described.

RNA isolation and real-time quantitative reverse transcription polymerase chain reaction

Corpus callosum was dissected from whole brains under a light microscope. Total RNA was then extracted from the tissue using the RNeasy® Mini Kit (Qiagen) as previously described (Gudi *et al*., 2011; Skripuletz *et al*., 2011*b*). The RNA concentration was measured with a NanoDrop 1000 device (Thermo Fisher Scientific). Complementary DNA was synthesized using the High Capacity cDNA Reverse Transcription Kit (Applied Biosystems). Real-time quantitative reverse transcription PCR analysis was performed using the StepOne™ Real-Time PCR System and appropriate TaqMan® probes (Applied Biosystems). All primers were exon-spanning. Gene expressions of CCL2, CCL3, CXCL10, CXCL12 and CXCL13 were analysed in the corpus callosum after 3 weeks of cuprizone treatment in transgenic and wild-type mice treated with ganciclovir or PBS and in age-matched normal-fed control mice (transgenic mice treated with ganciclovir or PBS, wild-type mice treated with PBS). The $\Delta\Delta$Ct method was used to determine differences in the expression between cuprizone-fed mice and age-matched control mice. Changes in messenger RNA expression levels were calculated after normalization to hypoxanthine phosphoribosyltransferase and glyceraldehyde 3-phosphate dehydrogenase.

Cell culture and enzyme-linked immunosorbent assay for measurement of CXCL10

Primary astrocyte cultures were prepared from 1- to 3-day-old Wistar rat cortices (Janvier) as previously described (Kipp *et al*., 2008; Braun *et al*., 2009). Twenty-four hours before astrocyte treatment, cultures were serum-deprived in Dulbecco's modified Eagle's medium containing 0.1% foetal calf serum. Cultures were treated with lipopolysaccharide (100 ng/ml, Sigma-Aldrich), tumour necrosis factor-α (100 ng/ml, Invitrogen), interferon-γ (100 U/ml, Peprotech), glutamate (4 μM, Sigma-Aldrich) or H_2O_2 (200 μM, Roth) for 24 h in Dulbecco's modified Eagle's medium without foetal calf serum. Previous studies revealed that the applied concentrations are sufficient to activate astrocytes, but are not toxic in the applied concentrations (Braun *et al*., 2009). CXCL10 protein levels were determined in the cell culture supernatant using a commercially available rat CXCL10 ELISA development kit (Peprotech) following the manufacturer's instructions. Protein content of cell pellets was quantified using the Bicinchoninic acid (BCA) Protein Assay Reagent Kit (Thermo Scientific) following the manufacturer's protocol.

Statistical analysis

Statistical analysis was performed using ANOVA followed by the Fisher's protected least significant difference test for *post hoc* comparison if appropriate. All data are given as arithmetic means ± standard error of the mean (SEM). *P*-values of the different ANOVAs are given in the results, and group comparisons derived from *post hoc* analysis are provided in the figures. In the latter case, significant effects are indicated by asterisks (*$P < 0.05$, **$P < 0.01$, ***$P < 0.001$).

Results

Astrocyte ablation during cuprizone-induced demyelination

The degree of astrogliosis during cuprizone-induced demyelination was analysed by GFAP immunostaining. Between wild-type C57BL/6 mice and GFAP–thymidine kinase transgenic mice fed with normal chow and injected with PBS or ganciclovir, no difference could be observed in the corpus callosum (Fig. 1) and cortex (Supplementary Fig. 2). These results indicate that ganciclovir treatment does not change astrogliosis in non-diseased mice brains.

During cuprizone feeding, there was a marked increase in GFAP-positive astrocytes in the corpus callosum (Fig. 1) and cortex (Supplementary Fig. 2) after only 3 weeks of treatment that remained at a high level after 4 and 5 weeks. In cuprizone-fed mice, no difference was visible between PBS-treated GFAP–thymidine kinase transgenic mice and wild-type C57BL/6 mice injected with PBS or ganciclovir. After injections of ganciclovir in cuprizone-fed GFAP–thymidine kinase transgenic mice, there was a strong loss of GFAP-positive astrocytes in both the corpus callosum and cortex (for both, $P < 0.0001$).

The extent of proliferating astrocytes was visualized by double staining for the marker Ki-67. In the corpus callosum, no or only few proliferating astrocytes were found in mice fed with normal chow and injected with PBS or ganciclovir (Fig. 1). During cuprizone treatment, the amount of proliferating astrocytes increased in PBS-treated GFAP–thymidine kinase transgenic mice and wild-type C57BL/6 mice injected with PBS or ganciclovir in a similar manner. In cuprizone-fed GFAP–thymidine kinase transgenic mice that were injected with ganciclovir, there was a strong loss of proliferating GFAP-positive astrocytes in the corpus callosum ($P < 0.0001$).

In the cerebral cortex, the amount of proliferating astrocytes was lower by a factor of ~25 as compared with the corpus callosum, which is in line with previous observations (Gudi *et al*., 2009). No differences between the groups were found (data not shown).

To confirm the degree of astrogliosis on cuprizone treatment and the loss of astrocytes in GFAP–thymidine kinase transgenic mice after ganciclovir treatment, additional immunostaining for the marker vimentin was performed. Double staining for the markers vimentin and GFAP showed that astrocytes express both markers in cuprizone-induced demyelination (for corpus callosum, representative images from Week 3 are shown in Fig. 2). Double staining for the markers vimentin and RCA-1 revealed that activated microglia do not express vimentin (Fig. 2).

Similar to the GFAP results, there was an increase in vimentin-positive astrocytes in the corpus callosum (Supplementary Fig. 3; $P < 0.0001$) and cortex (Supplementary Fig. 3; $P < 0.0001$) during demyelination. Ganciclovir injections in cuprizone-fed GFAP–thymidine kinase transgenic mice induced a strong loss of vimentin-positive astrocytes in both areas analysed and confirmed the results of GFAP staining. In the corpus callosum, the amount of vimentin-positive proliferating astrocytes increased in the three

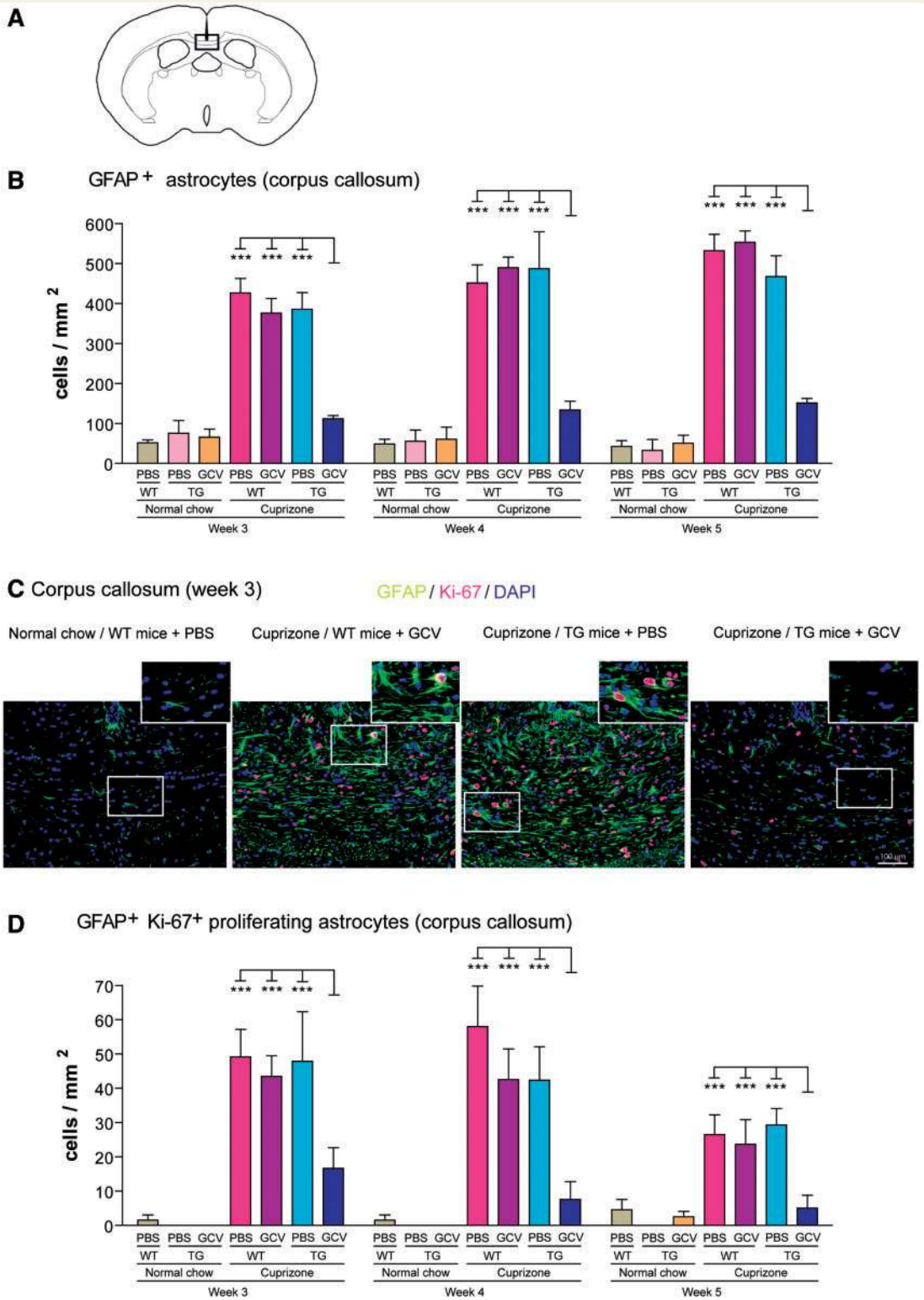

Figure 1 Astrocytes during cuprizone treatment in the corpus callosum. In the sketch of the mouse brain (**A**), the boxed area represents the area of the corpus callosum that was analysed. Graphs represent mean cell numbers from six animals per time point and group of GFAP-positive astrocytes in the corpus callosum (**B**) and GFAP/Ki-67 double-positive proliferating astrocytes in the corpus callosum (**D**). Significant effects between cuprizone groups are indicated by asterisks (***$P < 0.001$). In (**C**), representative brain sections stained for GFAP and Ki-67 are shown in the corpus callosum at Week 3 (nuclei were counterstained with DAPI). Each bar represents the mean ± SEM. GCV = ganciclovir; TG = GFAP–thymidine kinase transgenic mice; WT = wild-type mice.

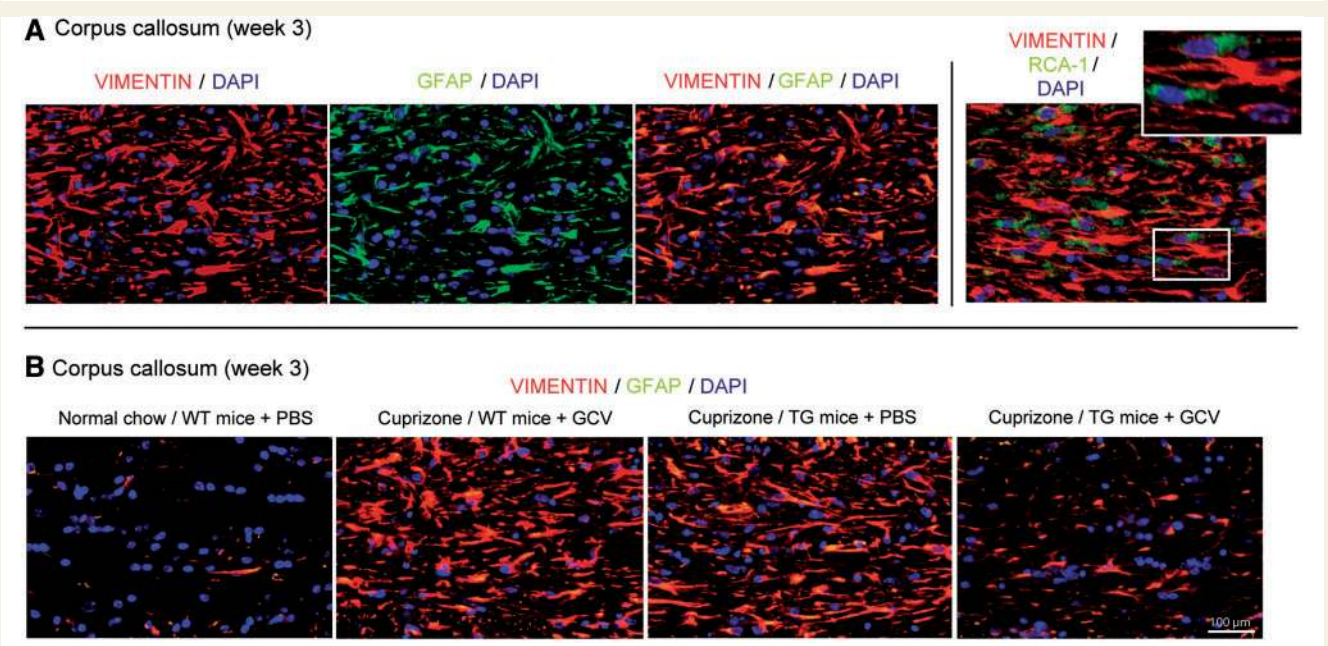

Figure 2 GFAP- and vimentin-positive astrocytes during cuprizone treatment in the corpus callosum. Single staining for the markers GFAP or vimentin and double staining for vimentin and GFAP show that astrocytes express both markers in cuprizone-induced demyelination (**A**). Double staining for the markers vimentin and RCA-1 show that activated microglia do not express vimentin (**A**). (**B**) Representative stained brain sections for vimentin and GFAP are shown in the corpus callosum at Week 3 of cuprizone exposure (nuclei were counterstained with DAPI). GCV = ganciclovir; TG = GFAP–thymidine kinase transgenic mice; WT = wild-type mice.

cuprizone control groups (GFAP–thymidine kinase transgenic mice injected with PBS and wild-type C57BL/6 mice injected with PBS or ganciclovir), whereas a strong loss occurred after ganciclovir injections in GFAP–thymidine kinase transgenic mice (Supplementary Fig. 3; $P < 0.0001$). Again, in the cerebral cortex, the proliferation rate of astrocytes was very low (only 0.5–2 cells/mm^2 were found), and thus no differences between the groups could be found (representative images in Supplementary Fig. 3D show the low proliferation activity of astrocytes in the cortex).

Astrocyte ablation inhibits cuprizone-induced loss of myelin

To evaluate whether astrocyte ablation affects toxin-induced demyelination, brain sections were analysed for the myelin markers myelin proteolipid protein, myelin oligodendrocyte glycoprotein and myelin-associated glycoprotein and the histochemical Luxol fast blue staining. Transgenic and wild-type mice fed with normal food and injected with PBS or ganciclovir showed normal myelin patterns in the corpus callosum (Fig. 3 and Supplementary Fig. 4) and cortex (Supplementary Fig. 5).

After 3 weeks of cuprizone feeding, loss of myelin began in the corpus callosum, as shown by myelin proteolipid protein (Fig. 3; $P < 0.0001$), myelin-associated glycoprotein (Supplementary Fig. 4; $P < 0.0001$), myelin oligodendrocyte glycoprotein (Supplementary Fig. 4; $P < 0.0001$) and Luxol fast blue staining (Supplementary Fig. 4; $P < 0.0001$). Demyelination continued during cuprizone administration and reached its maximal degradation after 5 weeks. No difference was found between wild-type C57BL/6 mice injected with PBS or ganciclovir and GFAP–thymidine kinase transgenic mice injected with PBS. Interestingly, in astrocyte-ablated GFAP–thymidine kinase transgenic mice, no or only slight demyelination was observed after 3 weeks of cuprizone treatment. At all time points investigated, demyelination was significantly diminished in GFAP–thymidine kinase transgenic mice after astrocyte ablation compared with the three cuprizone control groups.

In the cerebral cortex, similar results were found when compared with the corpus callosum. In ganciclovir-treated GFAP–thymidine kinase transgenic mice, there was a significantly reduced demyelination of the cerebral cortex after 3, 4 and 5 weeks for myelin proteolipid protein (Supplementary Fig. 5; $P < 0.0001$) and myelin-associated glycoprotein (Supplementary Fig. 5; $P < 0.0001$) staining compared with the three cuprizone control groups (GFAP–thymidine kinase transgenic mice injected with PBS and wild-type C57BL/6 mice injected with PBS or ganciclovir). Brain sections stained with Luxol fast blue and myelin oligodendrocyte glycoprotein were not investigated for cortical demyelination because of the low sensitivity of Luxol fast blue and myelin oligodendrocyte glycoprotein to demonstrate cortical myelin (Skripuletz *et al.*, 2008; Gudi *et al.*, 2009).

Astrocyte ablation does not change cuprizone-induced loss of oligodendrocytes

Mature oligodendrocytes were visualized using immunohistochemical staining for Nogo-A and APC. No effects on oligodendrocyte numbers were found in GFAP–thymidine kinase transgenic mice

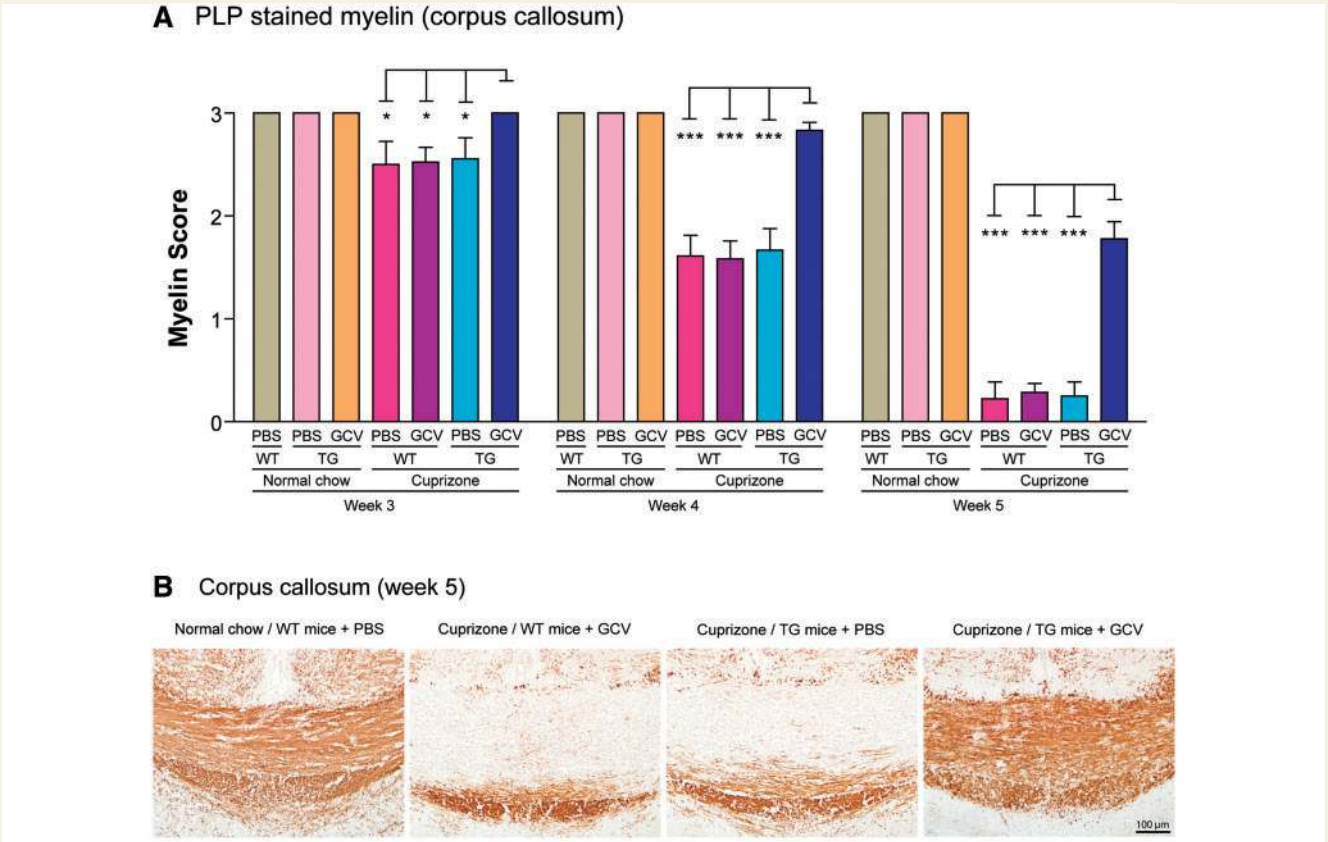

Figure 3 Course of demyelination in the corpus callosum. The extent of demyelination was judged by scoring of myelin proteolipid protein (PLP) (**A**). Brain sections were scored in a blinded manner by three independent observers. Score of 3 represents complete myelination, whereas score of 0 represents complete demyelination. Significant effects between cuprizone groups are indicated by asterisks (*$P < 0.05$, ***$P < 0.001$). In (**B**), representative brain sections stained for myelin proteolipid protein are shown in the corpus callosum at Week 5. Each bar represents the mean ± SEM. GCV = ganciclovir; TG = GFAP–thymidine kinase transgenic mice; WT = wild-type mice.

and wild-type C57BL/6 mice fed with normal chow and injected with PBS or ganciclovir in both the corpus callosum and cortex (Fig. 4 and Supplementary Fig. 6).

In the corpus callosum, a severe loss of mature oligodendrocytes was detectable after cuprizone feeding. Nogo-A- (Fig. 4) and APC-positive (Supplementary Fig. 6) oligodendrocytes were nearly completely depleted in all cuprizone-fed mice (GFAP–thymidine kinase transgenic mice and wild-type C57BL/6 mice injected with PBS or ganciclovir) after 3 and 4 weeks of treatment. This result is of particular interest, as it does not show any difference between the transgenic and wild-type mice, implicating that loss of astrocytes does not prevent cuprizone-induced damage/loss of mature oligodendrocytes.

In accordance with previous results, oligodendrocytes began to reappear at Week 5 (Skripuletz *et al*., 2011*b*). The density of newly generated Nogo-A- (Fig. 4) and APC-positive (Supplementary Fig. 6) cells was significantly lower in GFAP–thymidine kinase transgenic mice treated with ganciclovir as compared with PBS-treated GFAP–thymidine kinase transgenic mice and wild-type C57BL/6 mice injected with PBS or ganciclovir.

Similar to the corpus callosum, a severe loss of mature oligodendrocytes occurred in the cerebral cortex after animals were fed cuprizone. Nogo-A- and APC-positive (Supplementary Fig. 6) oligodendrocytes were almost completely depleted during demyelination at Weeks 3, 4 and 5 in all cuprizone-fed mice (GFAP–thymidine kinase transgenic mice injected with PBS and wild-type C57BL/6 mice injected with PBS or ganciclovir). In previous studies, we demonstrated that new oligodendrocytes reappear not earlier than at Week 6 in the cortex (Skripuletz *et al*., 2011*b*). Analogous to the corpus callosum, astrocyte ablation in GFAP–thymidine kinase transgenic mice did not influence cuprizone-induced loss of mature oligodendrocytes in the cortex.

In the cuprizone model, oligodendrocyte death and downregulation of myelin genes are already present 3–7 days after the start of cuprizone treatment and weeks before demyelination is visible in the corpus callosum (Morell *et al*., 1998; Komoly, 2005; Hesse *et al*., 2010). We confirmed these observations by additional immunohistochemical double stainings for oligodendroglia (Nogo-A, APC) and myelin markers (myelin basic protein, myelin-associated glycoprotein, CNPase). After 3 weeks of cuprizone exposure, mature oligodendrocytes had nearly completely disappeared despite remaining myelin protein expression as shown by myelin basic protein, myelin-associated glycoprotein and CNPase stainings (Fig. 5).

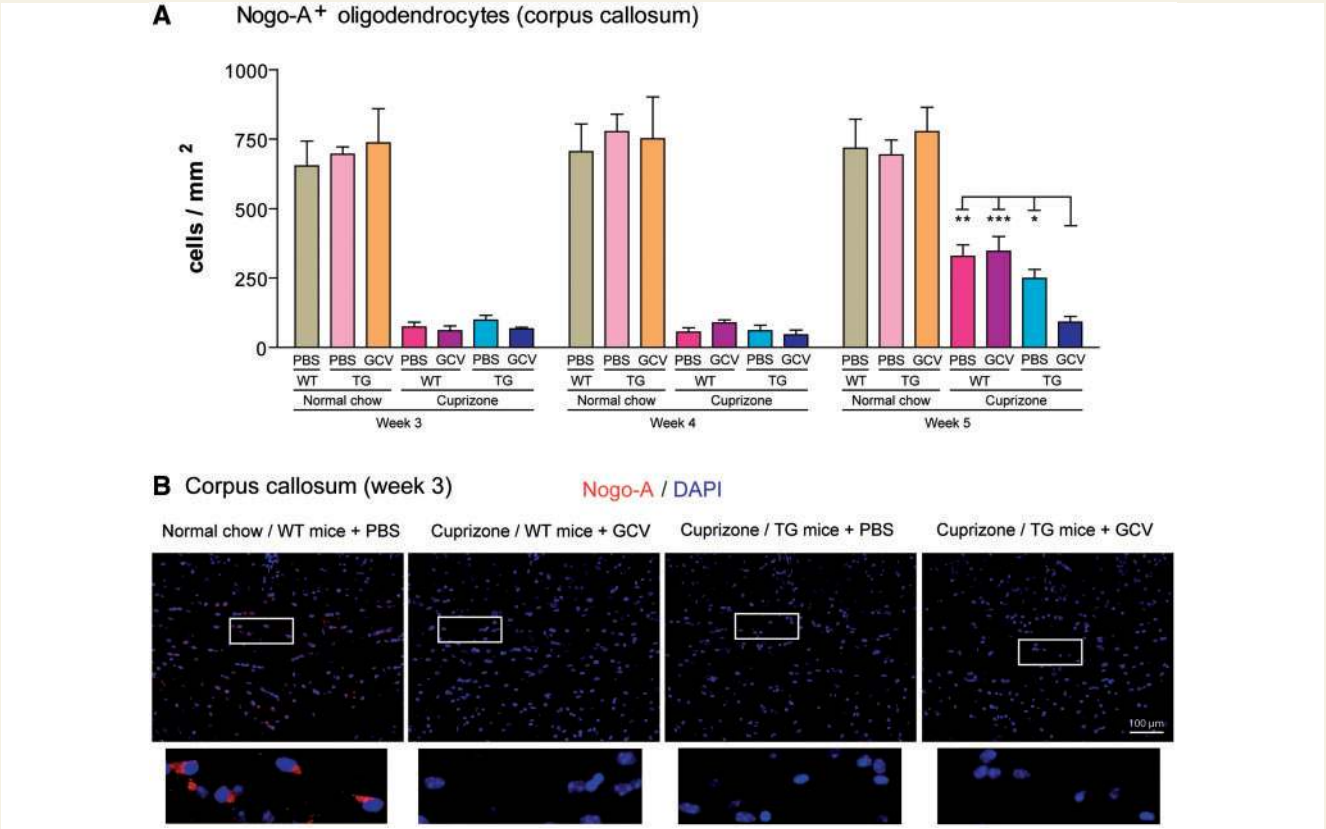

Figure 4 Mature oligodendrocytes during cuprizone treatment in the corpus callosum and cerebral cortex. Graphs represent mean cell numbers per time point and group of Nogo-A-positive oligodendrocytes in the corpus callosum (**A**) and cortex (**C**). Significant effects between cuprizone groups are indicated by asterisks (*$P < 0.05$, **$P < 0.01$, ***$P < 0.001$). In (**B**), representative brain sections stained for Nogo-A are shown in the corpus callosum at Week 3 (nuclei were counterstained with DAPI). Each bar represents the mean ± SEM. GCV = ganciclovir; TG = GFAP–thymidine kinase transgenic mice; WT = wild-type mice.

Furthermore, in all cuprizone groups, including astrocyte-ablated animals, there was a marked deficiency of interfascicular oligodendrocytes in the corpus callosum as shown by haematoxylin and eosin staining (Fig. 5). In the corpus callosum of normal-fed animals, interfascicular oligodendrocytes were found lying in rows side by side amongst the white matter nerve fibres. The loss of interfascicular oligodendrocytes in all cuprizone-fed groups confirms the immunohistochemical stainings for mature oligodendrocytes and shows that astrocyte ablation does not protect from oligodendroglial cell death in our model.

Astrocyte loss–induced preservation of myelin does not protect from axonal damage

To evaluate whether the remaining myelin after astrocyte ablation affects axons, brain sections were analysed to detect axonal damage.

First, axonal damage was analysed by quantification of APP-positive axons in the corpus callosum after 5 weeks of cuprizone exposure, the time point of maximal myelin degradation in cuprizone control mice (wild-type C57BL/6 mice injected with PBS or ganciclovir and GFAP–thymidine kinase transgenic mice injected with PBS) and the time point of preserved myelin in astrocyte-ablated GFAP–thymidine kinase transgenic mice. As shown in Fig. 6, the amount of APP-positive axons was increased after 5 weeks of cuprizone exposure. No difference was found between cuprizone groups, indicating that the remaining myelin in astrocyte-ablated animals did not protect from axonal damage.

Second, staining for synaptophysin was performed to analyse axonal damage. Synaptophysin, a major synaptic vesicle membrane protein, is transported along the axon in an anterograde manner comparable with APP transport (Koo *et al*., 1990; Okada *et al*., 1995). Axonal transport disturbances and axon transection lead to accumulation of synaptophysin in spheroid formations similar to the typical axonal swelling as shown by APP staining (Katsuse *et al*., 2003; Creed *et al*., 2011; Schirmer *et al*., 2012). In our study, synaptophysin-positive axons were found in the corpus callosum after 5 weeks of cuprizone feeding (Fig. 6). The results confirmed those found in the APP staining, as no difference was found for axonal damage between cuprizone groups.

Additional double stainings for APP and the myelin marker proteolipid protein, and synaptophysin and proteolipid protein, show axonal damage despite preserved myelin (Fig. 6C). These results indicate that the function of myelin is lost in astrocyte-ablated animals.

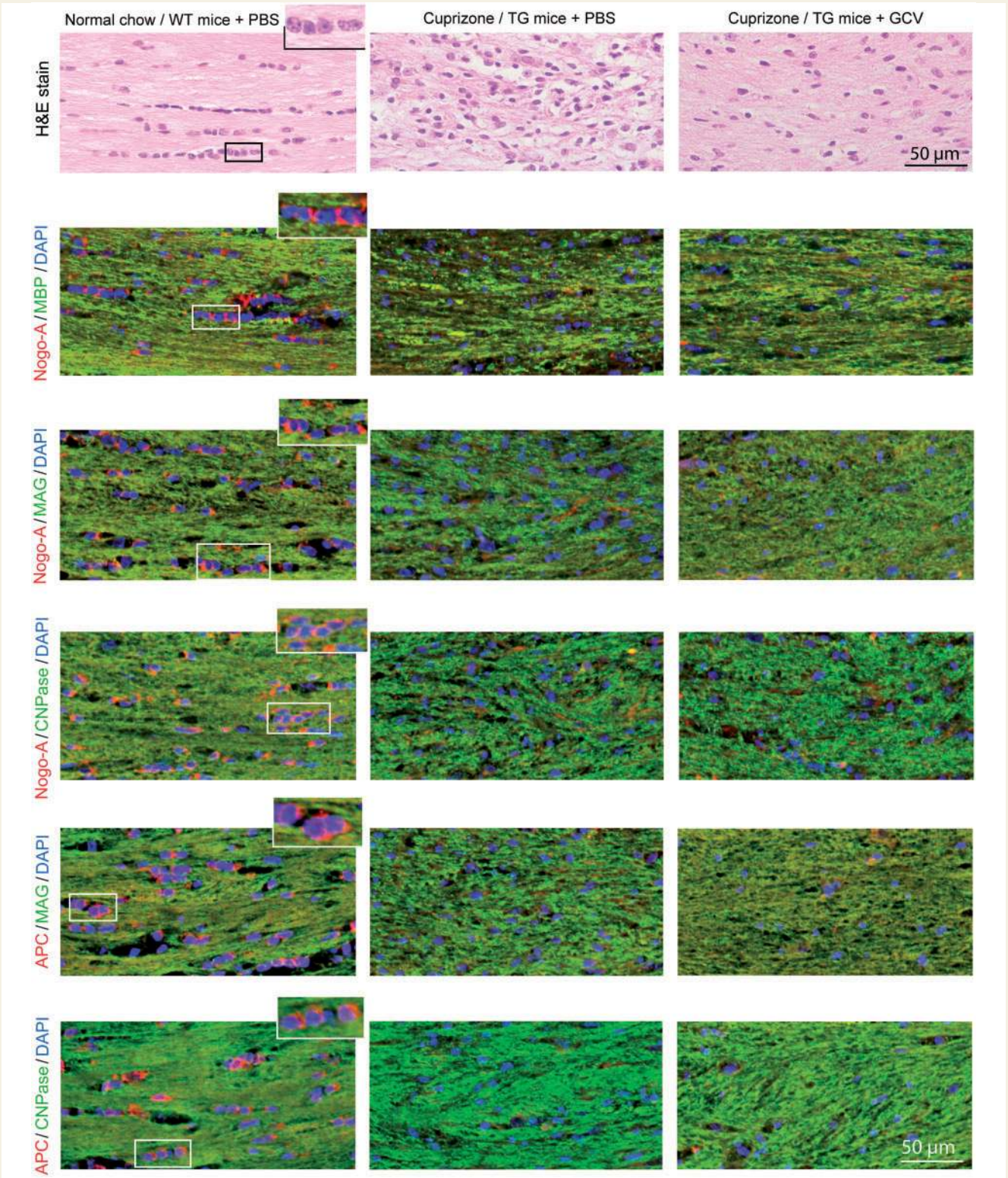

Figure 5 Haematoxylin and eosin stain (H&E) was performed to present interfascicular oligodendrocytes in normal-fed control mice. During cuprizone treatment, there was a marked deficiency of interfascicular oligodendrocytes in all cuprizone groups, including astrocyte-ablated animals, in the corpus callosum. In the figure, representative stained brain sections are shown in the corpus callosum at Week 3 (nuclei were counterstained with DAPI). Additional immunohistochemical double stainings for oligodendroglial marker and myelin marker (Nogo-A/myelin basic protein, Nogo-A/myelin-associated glycoprotein, Nogo-A/CNPase, APC/myelin-associated glycoprotein, APC/CNPase) were performed. After 3 weeks of cuprizone exposure, mature oligodendrocytes have nearly completely disappeared despite remaining myelin protein expression as shown by myelin basic protein, myelin-associated glycoprotein and CNPase stainings. GCV = ganciclovir; TG = GFAP–thymidine kinase transgenic mice; WT = wild-type mice.

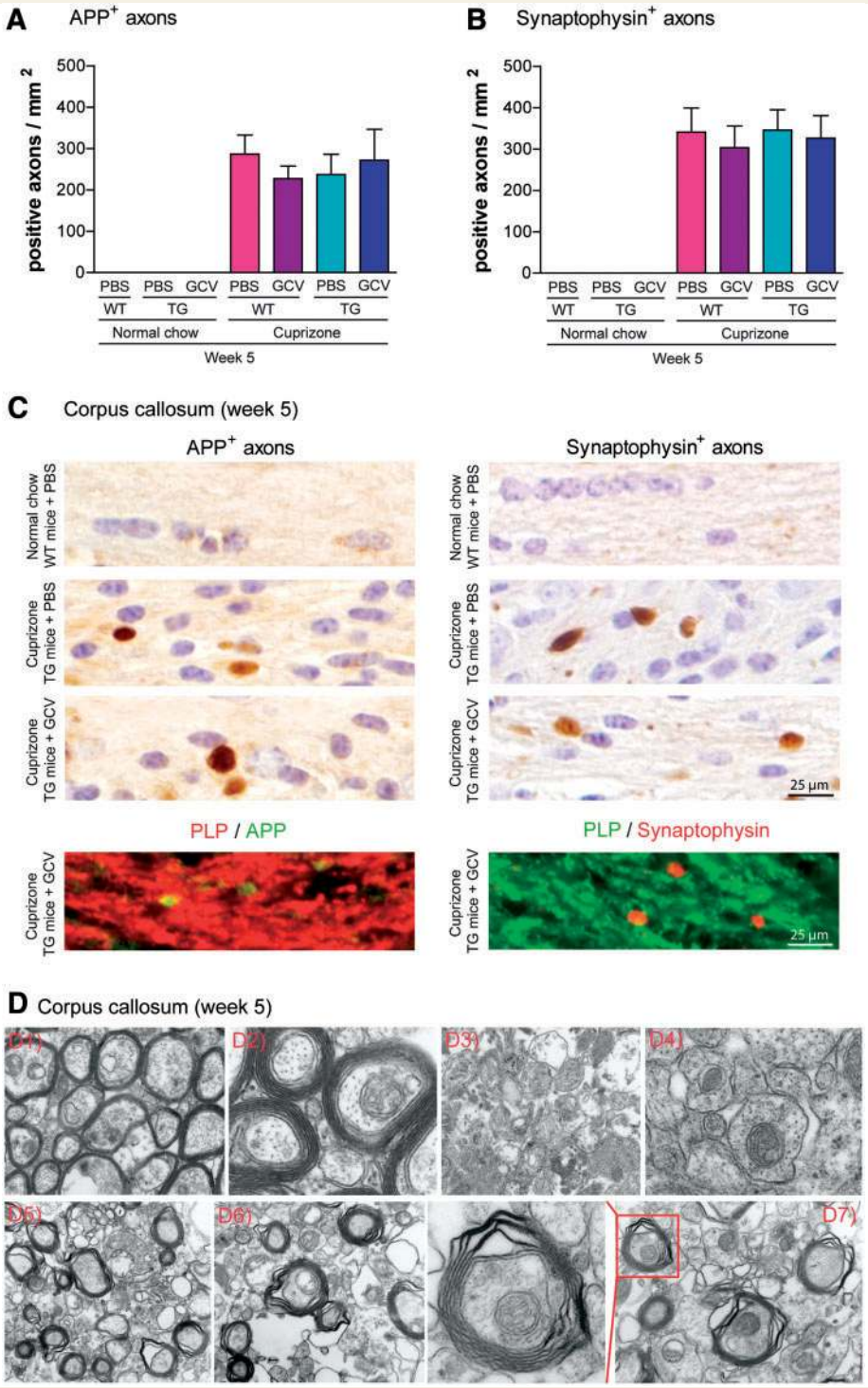

Figure 6 Axonal damage occurs despite preserved myelin at Week 5 of cuprizone feeding. Axonal damage was analysed by immunohistochemical stainings for APP and synaptophysin. Graphs represent mean cell numbers ± SEM per group of (**A**) APP- and (**B**) synaptophysin-positive axons in the corpus callosum. In (**C**), representative brain sections stained for APP and synaptophysin are shown in the corpus callosum at Week 5 (nuclei were counterstained with Mayer's haemalum solution). Double stainings for APP and proteolipid protein as well as synaptophysin and proteolipid protein show axonal damage despite preserved myelin (**C**). Ultrastructural analyses were performed to show myelinated axons in the corpus callosum. Representative brain sections are shown in the corpus callosum of control wild-type C57BL/6 mice fed with normal chow (**D1** and **D2**) and of cuprizone-fed mice at Week 5 (**D3** and **D4**: wild-type C57BL/6 mice injected with PBS; **D5–7**: GFAP–thymidine kinase transgenic mice after astrocyte ablation). Wild-type mice show nearly complete demyelination (**D3** and **D4**), whereas after astrocyte ablation, many axons remained myelinated (**D5–7**). The myelinated axons present disturbed myelin structure such as splits, sheath breakdown and vacuolated formations. GCV = ganciclovir; TG = GFAP–thymidine kinase transgenic mice; WT = wild-type mice.

Astrocyte ablation does not prevent myelin damage but inhibits the clearance of myelin debris

The discrepancy between preserved myelin despite oligodendrocyte and axonal damage led to electron microscopy studies to evaluate whether astrocyte loss affects myelin integrity on the ultrastructural level.

The three cuprizone groups with extensive reactive astrogliosis (wild-type C57BL/6 mice injected with PBS or ganciclovir and GFAP–thymidine kinase transgenic mice injected with PBS) showed nearly complete demyelination of axons after 5 weeks of cuprizone feeding (only 0–3% of axons remained myelinated; Fig. 6D). In contrast, after ablation of astrocytes in the GFAP–thymidine kinase transgenic mice, many axons remained myelinated (31–42% of axons remained myelinated; Fig. 6D). However, the majority of myelin sheaths presented an altered myelin structure. The circumferential outlines of these myelin lamellae were irregular. The myelin sheaths displayed splits, sheath breakdown and vacuolated formations. These ultrastructural examinations revealed that myelin damage did occur in astrocyte-depleted brains of GFAP–thymidine kinase transgenic mice, but without clearance of the altered myelin.

Recruitment of microglia is decreased after astrocyte loss

Accumulation of activated microglia was investigated by RCA-1 and Mac-3 stainings. The whole population of microglia was investigated with the marker Iba-1, which also stains resting microglia. No activated microglia were found in transgenic and wild-type mice fed with normal chow and injected with PBS or ganciclovir, either in the corpus callosum (Fig. 7) or in the cortex (Supplementary Fig. 7). Iba-1-positive microglia were found in mice fed with normal chow, but no difference between the groups could be observed (Supplementary Fig. 8).

In the corpus callosum and cortex, numbers of RCA-1- (Fig. 7 and Supplementary Fig. 7; for both, $P < 0.0001$), Mac-3- (data not shown; for both, $P < 0.0001$) and Iba-1-positive (Supplementary Fig. 8; for both, $P < 0.0001$) microglia increased strongly after 3 weeks of cuprizone treatment and reached a peak after 4 weeks in wild-type animals, whereupon a decrease occurred. No difference was found between wild-type C57BL/6 mice injected with PBS or ganciclovir and GFAP–thymidine kinase transgenic mice injected with PBS.

However, when GFAP–thymidine kinase transgenic mice were treated with ganciclovir, numbers of RCA-1-, Mac-3- and Iba-1-positive microglia were significantly decreased compared with the three cuprizone control groups after Weeks 3, 4 and 5 in both the corpus callosum and cortex.

To determine the activation state of microglia during demyelination, brain sections stained with Luxol fast blue/periodic acid–Schiff were analysed. Periodic acid–Schiff-positive material in microglia is well described as an indicator of myelin phagocytosis (Bitsch *et al*., 2000; Lin *et al*., 2005; Skripuletz *et al*., 2008; Kondo *et al*., 2011). In the corpus callosum and cortex, accumulation of periodic acid–Schiff-positive microglia began after 3 weeks of cuprizone diet and peaked after 4 weeks, similar to the RCA-1, Mac-3, and Iba-1 staining. In astrocyte-ablated GFAP–thymidine kinase transgenic mice, microglia containing periodic acid–Schiff-positive products of myelin degradation were also found, indicating that despite astrocyte loss, microglia were able to phagocytose (representative images are shown in Supplementary Fig. 9). Thus, the decreased myelin debris removal is rather the result of the reduced microglia recruitment into the lesion.

Effect of astrocyte ablation correlates with microglia activation

In two additional experimental settings, ganciclovir treatment was started at Week 3 (beginning of microglial recruitment and demyelination) or Week 4 (peak of microglial recruitment and presence of strong demyelination).

When ganciclovir treatment was started at Week 3 of cuprizone treatment, demyelination in the corpus callosum and cortex was significantly diminished compared with the three cuprizone control groups, as shown by proteolipid protein staining at Week 5 (Fig. 8A–C; corpus callosum, $P < 0.0001$; cortex, $P = 0.001$). Accordingly, no differences were found between wild-type C57BL/6 mice injected with PBS or ganciclovir and GFAP–thymidine kinase transgenic mice injected with PBS.

When ganciclovir treatment was started at Week 4 of cuprizone treatment, astrocyte ablation, in turn, did not influence demyelination in the corpus callosum nor in the cortex (Fig. 8D–F). At Week 5, complete demyelination occurred in the corpus callosum and strong demyelination occurred in the cortex in all cuprizone groups, showing no difference between groups (C57BL/6 mice injected with PBS or ganciclovir and GFAP–thymidine kinase transgenic mice injected with PBS or ganciclovir). These results indicate that astrocyte ablation at Week 4 cannot influence demyelination when microglia are already recruited and there is prominent microgliosis.

Astrocyte ablation decreases messenger RNA expression of CXCL10

To further identify factors involved in attracting microglia to demyelinating lesions, the messenger RNA expression of selected chemokines that have been associated with microglial recruitment was analysed.

After 3 weeks of cuprizone feeding when microglial recruitment started, the expression of CXCL10 was found to be strongly upregulated in wild-type C57BL/6 mice injected with PBS or ganciclovir and GFAP–thymidine kinase transgenic mice injected with PBS (Fig. 9; $P < 0.001$). In GFAP–thymidine kinase transgenic mice injected with ganciclovir, a significantly reduced expression of CXCL10 was found compared with the three cuprizone control groups, suggesting that astrocytes are the major source of CXCL10 messenger RNA expression in cuprizone-induced demyelination. Immunohistochemical stainings for CXCL10 were performed to confirm the cellular source of this chemokine. Indeed, the cells producing CXCL10 showed astrocytic shape, and double

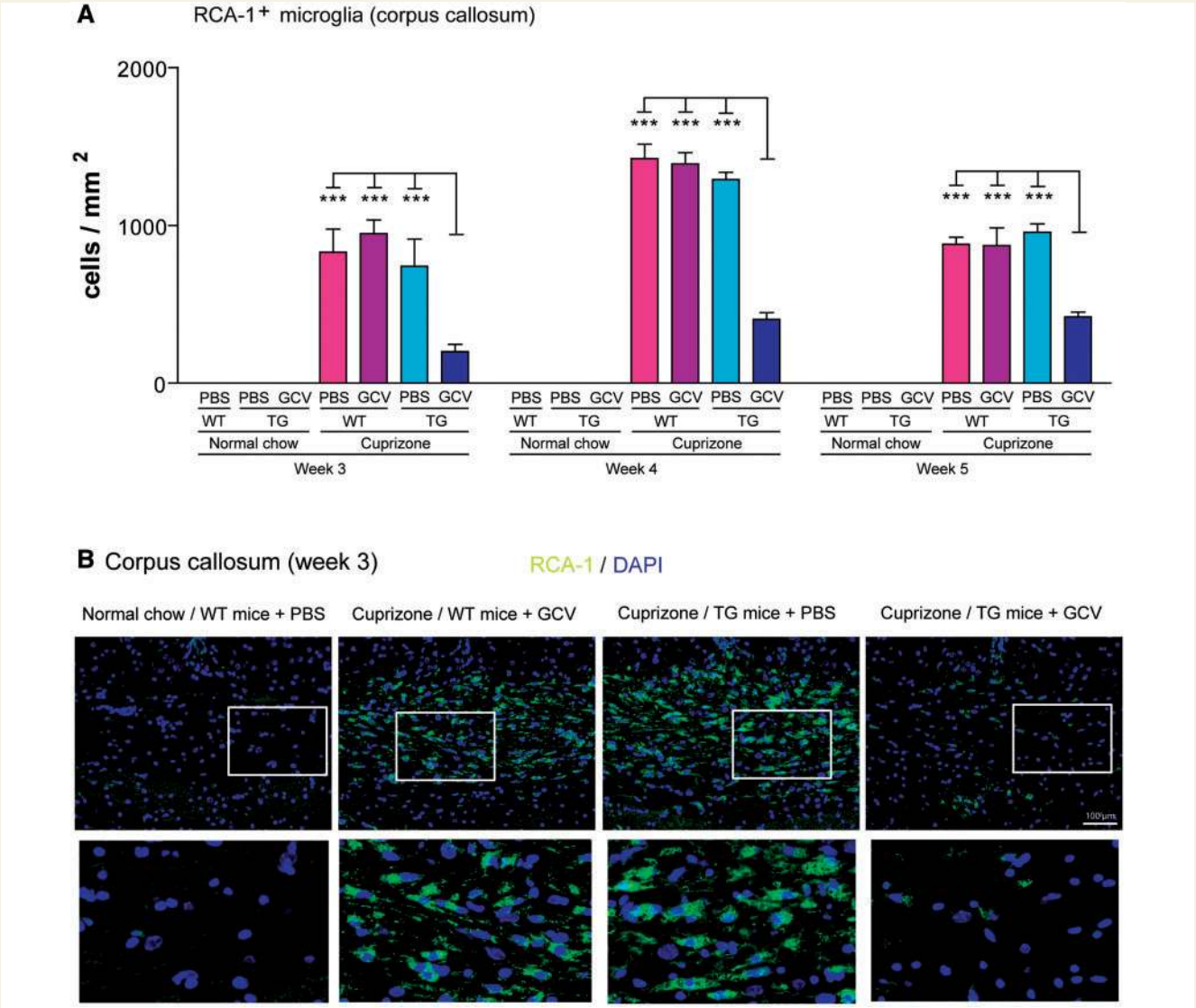

Figure 7 Activated microglia during cuprizone treatment in the corpus callosum. Graphs represent mean cell numbers per time point and group of RCA-1-positive microglia in the corpus callosum (**A**). Significant effects between cuprizone groups are indicated by asterisks (***$P < 0.001$). (**B**) Representative brain sections stained for RCA-1 are shown in the corpus callosum at Week 3 (nuclei were counterstained with DAPI). Each bar represents the mean ± SEM. GCV = ganciclovir; TG = GFAP–thymidine kinase transgenic mice; WT = wild-type mice.

stainings with GFAP confirmed this (Fig. 9). Double stainings with the microglia marker RCA-1 showed no co-localization of CXCL10 in these cells (Fig. 9).

To further confirm the secretion of CXCL10 in astrocytes, additional cell culture experiments were performed. In astrocytes stimulated with lipopolysaccharide, interferon-γ or tumour necrosis factor-α, there was a significantly increased secretion of CXCL10 compared with control ones (Supplementary Fig. 10; $P < 0.0001$). These *in vitro* data support the *in vivo* finding that astrocytes produce CXCL10.

The messenger RNA expression of *CCL2* and *CCL3* was found to be strongly upregulated during cuprizone-induced demyelination in all cuprizone-fed groups (C57BL/6 mice injected with PBS or ganciclovir and GFAP–thymidine kinase transgenic mice injected with PBS or ganciclovir) as compared with mice fed with normal chow (data not shown). There was no difference after astrocyte ablation, indicating that astrocytes do not play a major role in providing these chemokines in this model.

CXCL12 and CXCL13 seem to have no influence in cuprizone-induced demyelination, as no difference in the messenger RNA expression was found in transgenic and wild-type mice fed with cuprizone or fed with normal chow (data not shown).

Decreased microgliosis after astrocyte ablation delays the clearance of myelin debris

As described earlier in the text, astrocyte ablation prevented myelin clearance in the corpus callosum and cortex through the

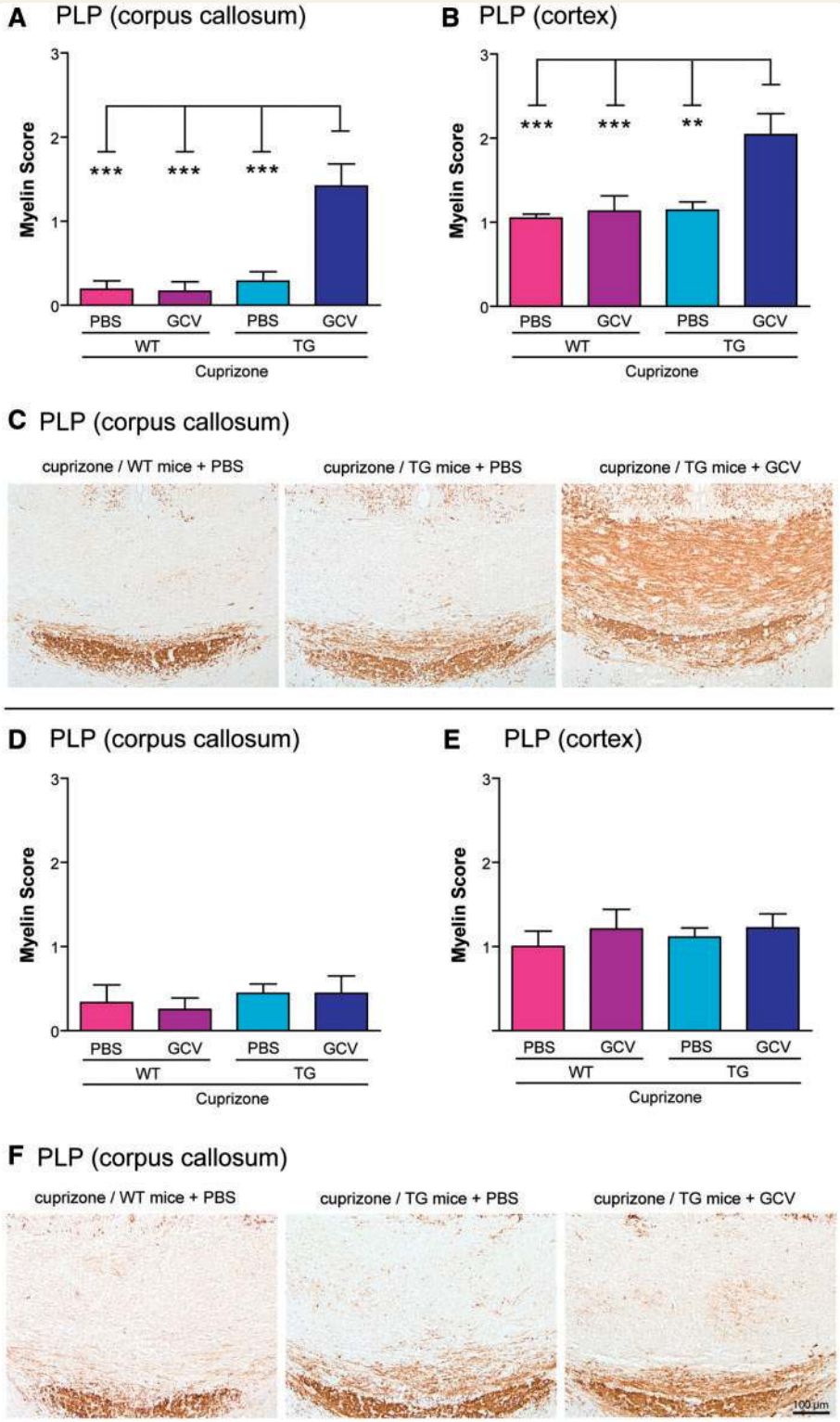

Figure 8 Course of demyelination in the corpus callosum and cortex during cuprizone treatment in response to late astrocyte ablation. In two experimental settings, astrocyte ablation was started at Week 3 (beginning of microglial recruitment and demyelination; **A–C**) or Week 4 (peak of microglial recruitment and presence of strong demyelination; **D–F**). The extent of demyelination was judged by scoring of proteolipid protein. Brain sections were scored in a blinded manner by three independent observers. A score of 3 represents complete myelination in the corpus callosum, and a score of 4 represents normal myelination in the cortex. A score of 0 represents complete demyelination in the corpus callosum and cortex. Significant effects between cuprizone groups are indicated by asterisks (**$P < 0.01$, ***$P < 0.001$). In (**C**) and (**F**), representative brain sections stained for proteolipid protein are shown in the corpus callosum at Week 5. Each bar represents the mean ± SEM. GCV = ganciclovir; TG = GFAP–thymidine kinase transgenic mice; WT = wild-type mice.

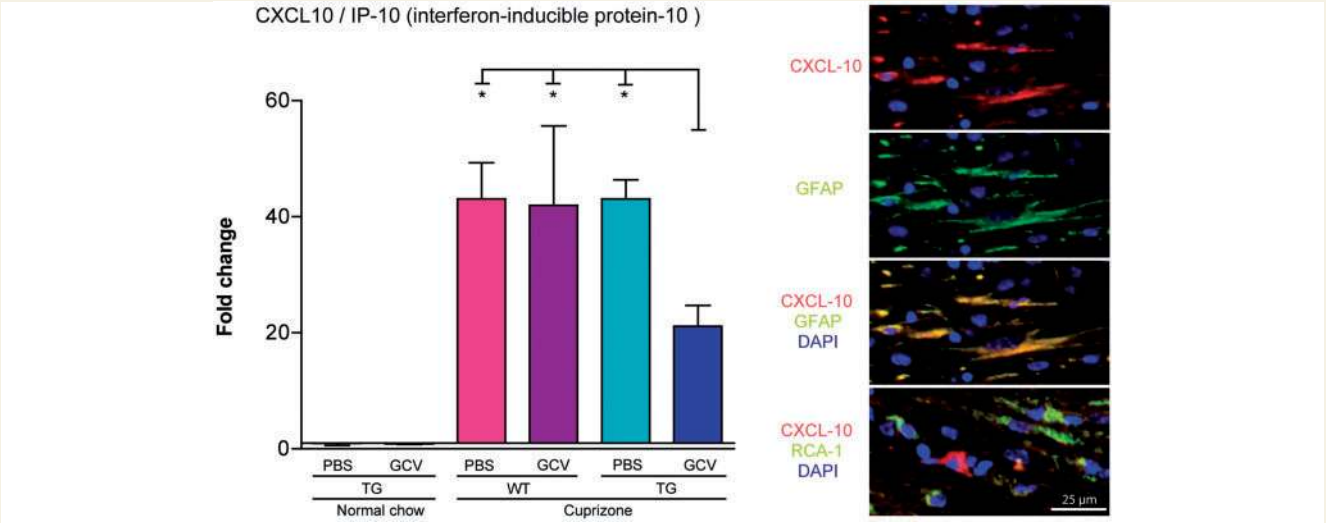

Figure 9 Expression of CXCL10 (interferon-inducible protein-10) messenger RNA in the corpus callosum at Week 3. Graphs show messenger RNA expression fold changes of CXCL10 compared with wild-type normal-fed control mice. Significant effects between cuprizone groups are indicated by asterisks (*$P < 0.05$). Double stainings with the markers CXCL10 and GFAP show that astrocytes express the chemokine CXCL10 in cuprizone-induced demyelination. Double stainings with the markers CXCL10 and RCA-1 show that activated microglia do not express CXCL10. Nuclei were counterstained with DAPI. Each bar represents the mean ± SEM. GCV = ganciclovir; TG = GFAP–thymidine kinase transgenic mice; WT = wild-type mice.

reduction of microglia recruitment to the lesion. Additional analyses revealed that the remaining myelin is damaged and does not prevent axonal damage. Thus, a further time point (Week 6) was investigated to analyse what happens with the damaged myelin in the astrocyte-ablated transgenic mice.

At Week 6 of cuprizone exposure, all myelin sheaths in the corpus callosum have been cleared in astrocyte-ablated transgenic mice, whereas in control mice (wild-type C57BL/6 mice injected with PBS or ganciclovir and GFAP–thymidine kinase transgenic mice injected with PBS), there already was remyelination. As shown by proteolipid protein, Luxol fast blue, myelin-associated glycoprotein and myelin oligodendrocyte glycoprotein staining, nearly complete demyelination could be observed in astrocyte-ablated mice (Fig. 10). Remyelination during continued cuprizone administration at Week 6 is well described (Matsushima and Morell, 2001; Gudi *et al.*, 2009). Only with myelin oligodendrocyte glycoprotein there was no significant difference between the groups in myelin protein re-expression, which is in accordance with previous studies and developmental myelination (first, myelin basic protein, followed by proteolipid protein and finally by myelin oligodendrocyte glycoprotein; Gudi *et al.*, 2009). This result indicates that the removal of damaged myelin was delayed as a consequence of astrocyte ablation, and that this process is required before remyelination can occur.

In contrast to the corpus callosum, demyelination of the cortex is delayed, and complete demyelination occurs 1 week later at the Week 6 time point in the cuprizone model (Skripuletz *et al.*, 2008; Gudi *et al.*, 2009). Accordingly, we found nearly complete demyelination, as shown by myelin proteolipid protein and myelin-associated glycoprotein staining, in the three cuprizone control groups (wild-type C57BL/6 mice injected with PBS or ganciclovir and GFAP–thymidine kinase transgenic mice injected with PBS; Supplementary Fig. 13). Interestingly, in astrocyte-ablated transgenic mice, higher amounts of myelin proteolipid protein and myelin-associated glycoprotein were found at Week 6 compared with the three cuprizone control groups, showing that myelin clearance is also delayed in the cortex (for both $P < 0.0001$).

Owing to regional differences, oligodendrocytes reappear first after Week 6 in the cortex, and thus, only low numbers of Nogo-A- and APC-positive oligodendrocytes were found in all cuprizone groups at week 6 (Supplementary Fig. 13).

Analysis of glial reactions at Week 6 showed that a strong loss of GFAP- and vimentin-positive astrocytes was still observed in the corpus callosum and cortex after injections of ganciclovir in cuprizone-fed GFAP–thymidine kinase transgenic mice (Supplementary Fig. 12 and 13; for all, $P < 0.0001$). At Week 6, microglia numbers (RCA-1-, Mac-3- and Iba-1-positive cells) decreased strongly compared with Week 5 in the corpus callosum and cortex in the cuprizone groups, and no difference between the groups was observed (Supplementary Fig. 12 and 13).

Astrocyte ablation inhibits the regeneration of oligodendrocytes and myelin

The numbers of Nogo-A- and APC-positive cells in the corpus callosum after 5 and 6 weeks of cuprizone treatment indicate a decreased regeneration of oligodendrocytes after astrocyte ablation (Figs 4, 10 and Supplementary Fig. 6).

To further evaluate the role of astrocytes in oligodendrocyte precursor cell proliferation, double staining for Olig-2 and Ki-67 was performed. On cuprizone-induced demyelination, the numbers of proliferating oligodendrocyte precursor cells increased in

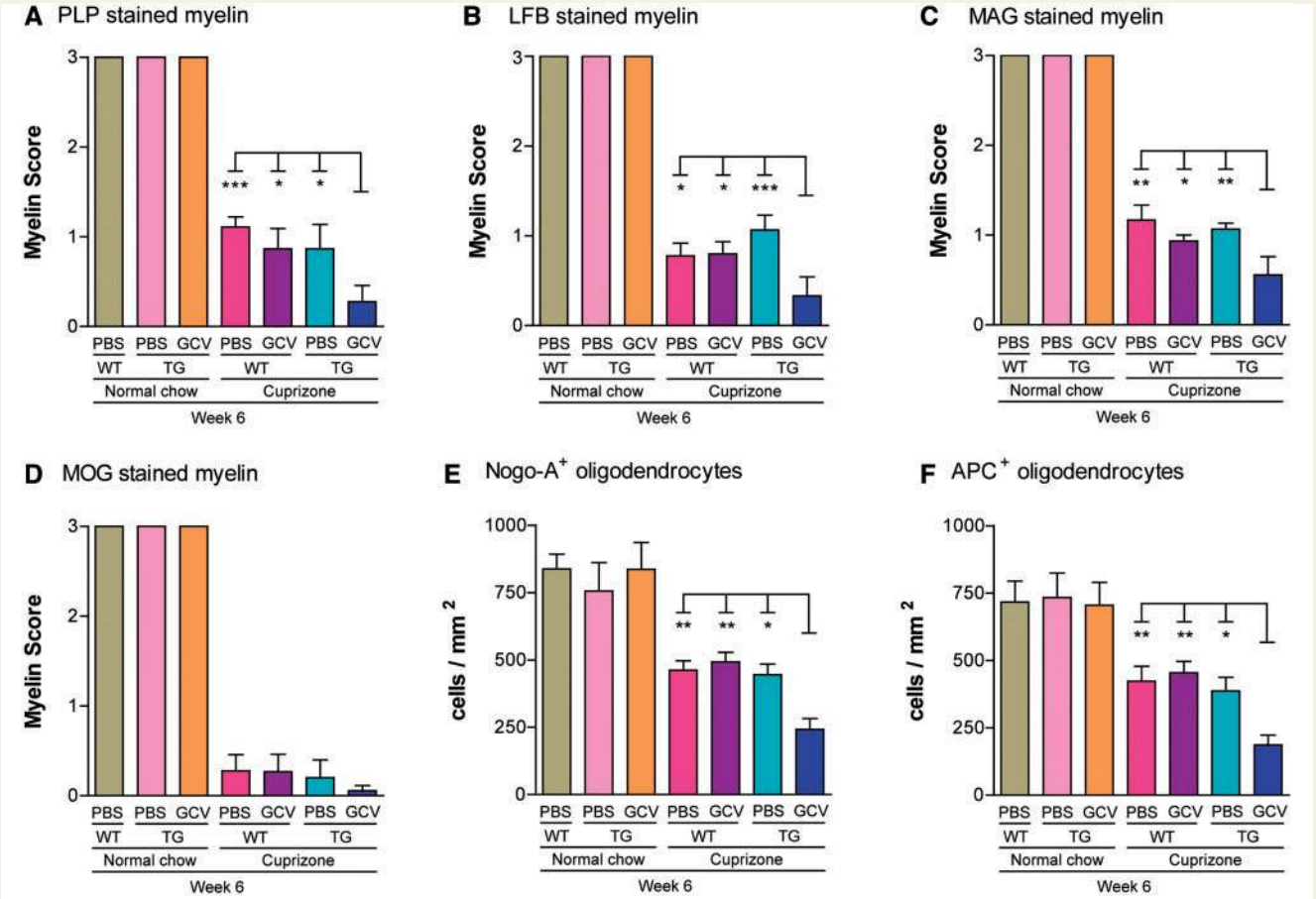

Figure 10 Myelin and oligodendrocytes after 6 weeks of cuprizone feeding in the corpus callosum. Corpus callosum was analysed for different myelin and oligodendroglial markers: proteolipid protein (**A**), Luxol fast blue (**B**), myelin-associated glycoprotein (**C**), myelin oligodendrocyte glycoprotein (**D**) and, for mature oligodendrocytes, Nogo-A (**E**) and APC (**F**). Each bar represents the mean ± SEM. Significant effects between cuprizone groups are indicated by asterisks (*$P < 0.05$, **$P < 0.01$, ***$P < 0.001$). GCV = ganciclovir; LFB = Luxol fast blue; MAG = myelin-associated glycoprotein; MOG = myelin oligodendrocyte glycoprotein; PLP = myelin proteolipid protein; TG = GFAP–thymidine kinase transgenic mice; WT = wild-type mice.

the three cuprizone control groups (wild-type C57BL/6 mice injected with PBS or ganciclovir and GFAP–thymidine kinase transgenic mice injected with PBS) and reached a peak after 4 weeks, followed by a decline in both areas analysed (Fig. 11, Supplementary Figs 11, 12 and 13). After astrocyte ablation in transgenic mice, the numbers of proliferating oligodendrocyte precursor cells were clearly reduced in the corpus callosum compared with the cuprizone control groups ($P < 0.0001$). In the cortex, reduced numbers of proliferating oligodendrocyte precursor cells were found in the astrocyte-ablated transgenic mice at the peak of proliferation (Week 4 of cuprizone feeding; $P < 0.0001$).

These results suggest that the loss of astrocytes negatively affects oligodendrocyte precursor cell proliferation and differentiation and leads to decreased remyelination. Because myelin debris is a potent inhibitor of remyelination by inhibiting oligodendrocyte precursor cell differentiation (Kotter *et al*., 2006), the delayed myelin clearance in astrocyte-ablated transgenic mice might inhibit oligodendrocyte precursor cell differentiation into oligodendrocytes and thus myelin regeneration. We therefore injected transgenic mice with ganciclovir, beginning at Week 4. As described earlier in the text, after 4 weeks of astrocyte loss, demyelination is not affected. This allowed investigation of remyelination without the inhibitory effects of remaining myelin debris. Mice were fed with cuprizone for up to 5 weeks, followed by 1 week of normal chow to allow remyelination. After 1 week on normal chow, strong remyelination was observed in the three cuprizone control groups, and no significant difference between these groups was found (Fig. 12). It was already described that the extent of myelin protein re-expression is extremely fast and robust in the corpus callosum in the cuprizone model (Matsushima and Morell, 2001; Lindner *et al*., 2008; Kipp *et al*., 2009; Skripuletz *et al*., 2011*a*). In contrast, transgenic mice after astrocyte ablation showed significantly reduced amounts of new myelin as shown by Luxol fast blue and proteolipid protein stainings compared with the cuprizone control groups ($P = 0.004$ for Luxol fast blue, $P < 0.0001$ for proteolipid protein; Fig. 12). Analogous to myelin re-expression, the density of Nogo-A-positive oligodendrocytes was significantly decreased in astrocyte-ablated transgenic mice compared with the three cuprizone control groups ($P < 0.001$; Fig. 12). These results show that astrocyte

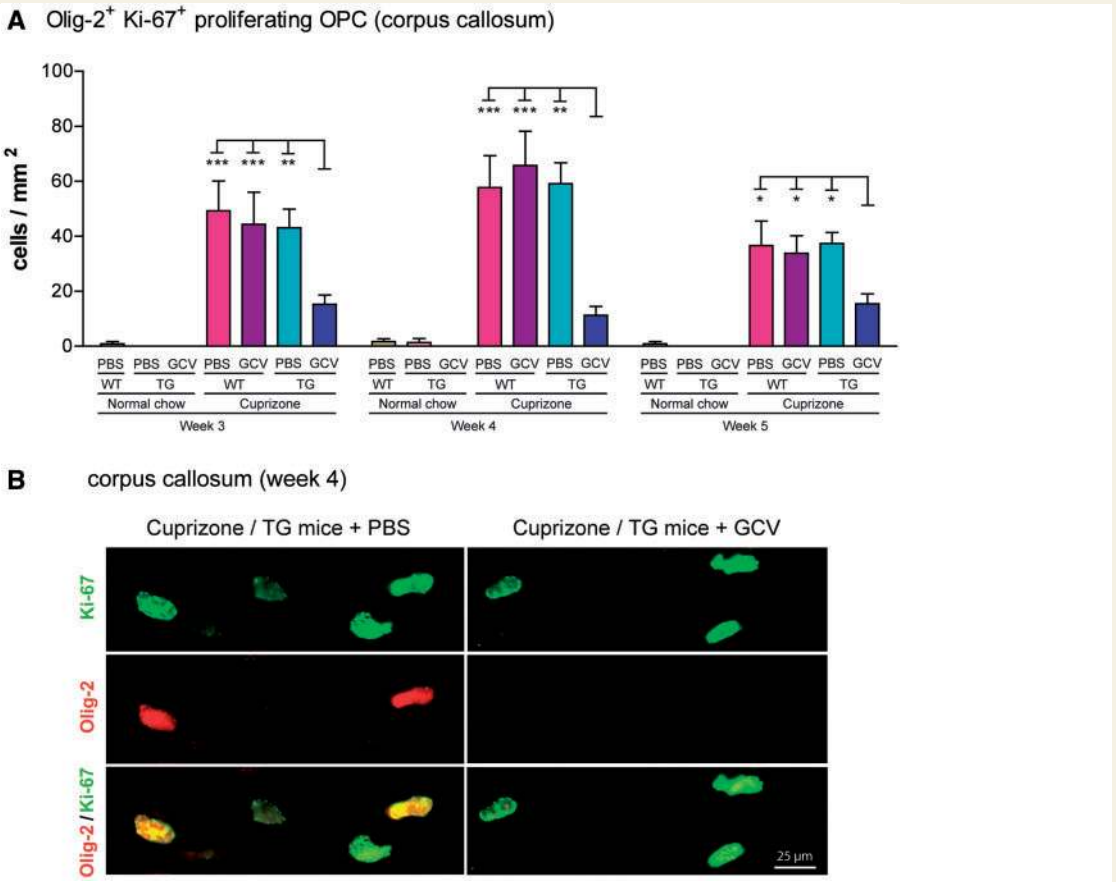

Figure 11 Proliferating oligodendrocyte precursor cells during cuprizone-induced demyelination. Graphs represent mean cell numbers per time point and group of Olig-2/Ki-67 double-positive proliferating oligodendrocyte precursor cells in the corpus callosum (**A**). Significant effects between cuprizone groups are indicated by asterisks (*$P < 0.05$, **$P < 0.01$, ***$P < 0.001$). (**B**) Representative brain sections stained for Olig-2- and Ki-67-positive cells are shown in the corpus callosum at Week 4. Each bar represents the mean ± SEM. GCV = ganciclovir; TG = GFAP–thymidine kinase transgenic mice; WT = wild-type mice.

loss exerts detrimental effects on remyelination via decreased numbers of oligodendrocytes.

Discussion

The aim of our study was to clarify the role of astrocytes in demyelinating diseases. We show here that astrocytes provide a signal environment that forms the basis for the recruitment of microglia and oligodendrocyte precursor cells that is required for successful remyelination.

The effects of astrocytes on CNS de- and remyelination were investigated in a well-described transgenic mouse model that enables the ablation of astrocytes as a consequence of ganciclovir treatment. This led to a loss of astrogliosis in both the grey and white matter in cuprizone-induced de- and remyelination.

Astrocytes regulate clearance of myelin debris

Interestingly, the extent of demyelination, as judged by histochemistry and immunohistochemistry, was significantly diminished in transgenic mice after astrocyte ablation as compared with the cuprizone control groups. However, reduction in mature oligodendrocyte numbers was not affected by the ablation of astrocytes, and axonal damage occurred to a similar extent in astrocyte-ablated animals as in the cuprizone control groups, indicating a loss of trophic support of the myelin. This discrepancy between oligodendrocyte and axonal damage and preserved myelin was resolved by additional ultrastructural analyses. Electron microscopy revealed that the ablation of astrocytes succeeded in higher numbers of myelinated axons; however, the structure of myelin was mostly disrupted. Thus, astrocyte ablation did not preserve myelin damage but inhibited the clearance of damaged myelin sheaths. This was associated by a reduced number of activated microglia in astrocyte-ablated transgenic mice, which alludes to a lack of microglia recruitment and phagocytosis of myelin debris.

Because the delay of myelin removal was accompanied by a distinct reduction of activated microglia in astrocyte-ablated animals, we analysed the time window of astrocyte effects on demyelination. In two different temporal injection protocols, astrocyte ablation was started at Week 3 (beginning of microglial

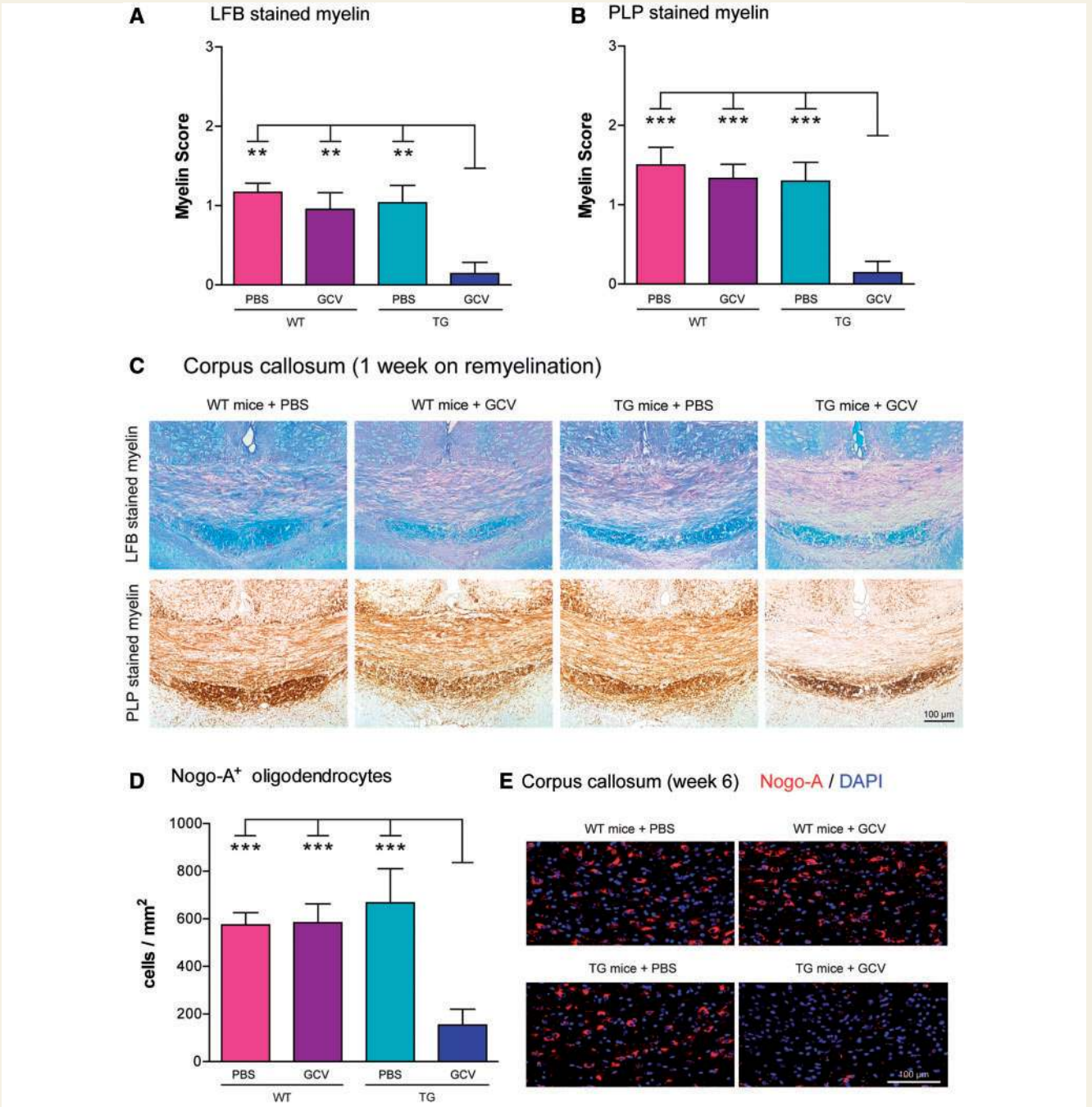

Figure 12 Remyelination and regeneration of oligodendrocytes in the corpus callosum 1 week after cuprizone withdrawal. The extent of remyelination was judged by scoring of Luxol fast blue (LFB; **A**) and proteolipid protein (PLP; **B**). Brain sections were scored in a blinded manner by three independent observers. A score of 3 represents complete myelination, and a score of 0 represents complete demyelination. In (**C**), representative brain sections stained for LFB and PLP are shown in the corpus callosum at Week 6 (1 week after remyelination). (**D**) Graph represents the mean cell numbers per group of Nogo-A-positive oligodendrocytes in the corpus callosum. (**E**) Representative brain sections stained for Nogo-A are shown in the corpus callosum at Week 6 (nuclei were counterstained with DAPI). Significant effects between cuprizone groups are indicated by asterisks (**$P < 0.01$, ***$P < 0.001$). Each bar represents the mean ± SEM. GCV = ganciclovir; TG = GFAP–thymidine kinase transgenic mice; WT = wild-type mice.

recruitment) or Week 4 (peak of microglial recruitment). Accordingly, ablation of astrocytes at the beginning of microglial recruitment resulted in decreased myelin removal in the corpus callosum and the cortex. When astrocyte ablation was started at the peak of microglia activation, there was no effect on myelin clearance. These different injection protocols illustrate that the recruitment of microglia and myelin removal depend on the presence of astrocytes.

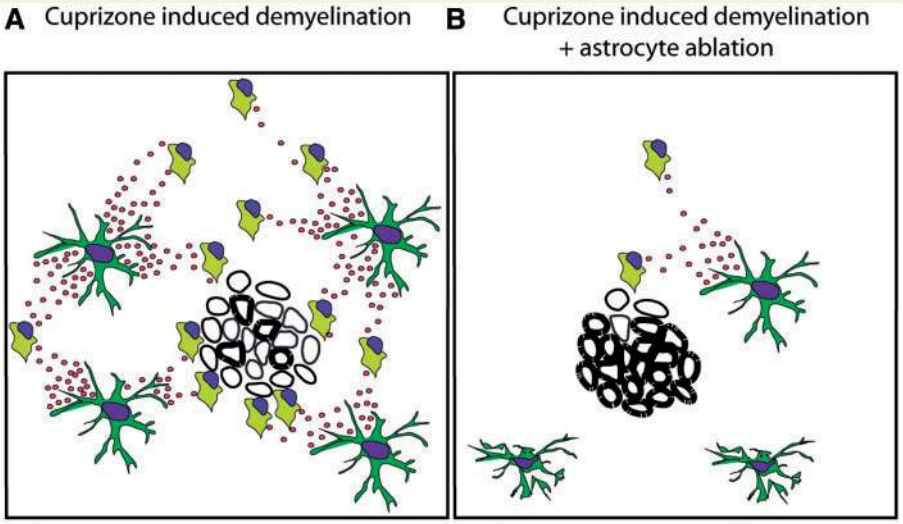

Figure 13 Schematic overview of astrocyte-mediated myelin clearance via recruitment of activated microglia to the lesion through upregulation of the chemokine CXCL10. In (**A**), reactive astrocytes secrete the chemokine CXCL10, which induces migration of microglia to cuprizone-damaged myelin lesions in the attempt to phagocytose the damaged myelin. In (**B**), reactive astrocytes were ablated using a transgenic mouse model during cuprizone-induced demyelination. The low numbers of astrocytes lead to a lower secretion of chemokines, and thus decreased recruitment of microglia. Lower microgliosis prevents from clearing the myelin debris. Thus, our results show that astrocytes exert beneficial effects in demyelinating diseases. Astrocytes are essential for demyelination through clearing the myelin debris by influencing the recruitment of microglia to damaged lesions.

Delayed removal of damaged myelin prevents early remyelination

When cuprizone was fed over a longer period, all myelin sheaths in the corpus callosum were cleared at Week 6 in astrocyte-ablated GFAP–thymidine kinase transgenic mice, indicating a delay in myelin debris clearance. While there is remyelination in wild-type mice at this time point, this was prevented in astrocyte-ablated transgenic mice by the delay in myelin removal. This illustrates the importance of myelin debris clearance for allowing remyelination and repair to occur. We think that this also holds true for repair processes in multiple sclerosis, where the myelin damaged by the immune response has to be cleared before remyelination can occur.

Astrocytes provide signals to attract microglia

Recruitment of activated microglia is a characteristic finding of most CNS autoimmune disorders, and both protective and detrimental functions have been proposed (Rasmussen *et al*., 2007; Simard and Rivest, 2007; Murphy *et al*., 2010). During demyelination, microglia exhibit an activated phenotype with a high phagocytic activity (Voss *et al*., 2012). Clearing damaged myelin presents an essential mechanism in demyelination, and it was shown that depletion of microglia/macrophages impaired myelin debris clearance, and thus demyelination and consequently remyelination (Kotter *et al*., 2006). There is increasing evidence that myelin clearance by microglia/macrophages is required for resolution of the inflammatory response and for efficient initiation of remyelination (Neumann *et al*., 2009). In particular, myelin debris was identified as an inhibitor of oligodendrocyte precursor cell differentiation (Kotter *et al*., 2006). Furthermore, microglia/macrophages containing myelin are known to contain anti-inflammatory molecules while lacking proinflammatory cytokines (Boven *et al*., 2006). Our data suggest that there is no clearance of disrupted myelin, a prerequisite for myelin repair when microglia are not recruited by astrocytes.

The role of astrocytes in demyelinating diseases is controversially discussed, and both protective and detrimental functions have been proposed (Nair *et al*., 2008; Moore *et al*., 2011). It was suggested that astrocytes are required for demyelination in the CNS by secreting a variety of factors, such as the chemokines CCL2, CCL3, CXCL10 and CXCL12, to attract inflammatory cells, such as microglia and macrophages, to the lesion (Babcock *et al*., 2003; El Hage *et al*., 2006; Bianchi *et al*., 2011; Qin and Benveniste, 2012). Thus, we analysed the messenger RNA expression of these chemokines in demyelinating lesions to identify astrocytic factors involved in the diminished microgliosis. Levels of CXCL10 messenger RNA expression were found to be strongly upregulated during demyelination in mice with normal astrocyte function, whereas in GFAP–thymidine kinase transgenic mice after astrocyte ablation, a significantly reduced expression of CXCL10 messenger RNA was found. Double immunofluorescence stainings revealed that CXCL10 was expressed in reactive astrocytes but not in activated microglia. The secretion of CXCL10 by astrocytes could be confirmed by additional *in vitro* experiments and was upregulated by interferon-γ, tumour necrosis factor-α or lipopolysaccharide.

A major role of astrocytes and CXCL10 in demyelinating diseases was already suggested by previous immunohistochemical

analyses on brain tissue from patients with multiple sclerosis (Tanuma *et al*., 2006). CXCL10 was found to be highly expressed at the rim of demyelinating plaques, and double immunofluorescence stainings showed that CXCL10 was expressed by astrocytes and not by microglia. This led to the suggestion that CXCL10 may be involved in migration and activation of microglia/macrophages. Our results confirm these observations by showing that the expression of CXCL10 is associated with astrocytes and is decreased after their ablation.

Astrocytes create a repair-permissive environment

A beneficial function of astrocytes has also been attributed to their ability to form glial scars, which limit CNS inflammation by constituting a physical barrier for inflammatory cells to enter demyelinated areas. In the immune-mediated animal model EAE, ablation of astrocytes in GFAP–thymidine kinase transgenic mice (as in our study) resulted in a disrupted formation of the glial scar, which was associated with an increased recruitment of peripheral inflammatory cells into the CNS, including T cells, neutrophils and macrophages (Voskuhl *et al*., 2009). In these mice, a more severe clinical EAE course was observed. Similar results were shown by another EAE study, in which the astrocyte-specific function of gp130 was analysed in GFAP-Cre gp130 mice (Haroon *et al*., 2011). Mice lacking the cell surface expression of gp130 developed a clinically more severe EAE, accompanied by larger areas of demyelination and increased numbers of CD4 T^+cells in the CNS. The results from different animal models show that astrocytes exert various parts of action in demyelination, and that it is not possible to uncover their complex pathobiology in demyelination by using only one animal model. To induce demyelination different myelin insults such as inflammation, toxins, viruses and genetic myelin mutations can be used (Schreiner *et al*., 2009). Because no animal model covers the complex pathomechanisms of human multiple sclerosis, the various animal models need to be used selectively to analyse different aspects of demyelination and remyelination in the attempt to fill gaps not presented by other models. The cuprizone model is particularly suitable to investigate remyelination without the possible interferences of peripheral immune cells such as macrophages and lymphocytes (Matsushima and Morell, 2001; Kipp *et al*., 2009; Skripuletz *et al*., 2011*a*). In addition to the role of astrocytes to provide the required signals to recruit microglia and thus allow the efficient removal of damaged myelin as a prerequisite for remyelination, we could demonstrate that astrocytes contribute to create a repair permissive environment during remyelination after the myelin debris has been removed. Astrocyte ablation at this time point impairs oligodendrocyte generation and formation of new myelin.

In conjunction with previous studies and our present data, we propose a dual beneficial mechanism of action for astrocytes on remyelination: regenerative effects by recruiting phagocytosing cells to clear damaged myelin, and regenerative effects by modulating the regeneration of oligodendrocyte precursor cells and thus oligodendrocytes.

Conclusion

In conclusion, we show that astrocytes are essential to activate microglia for removal of damaged myelin sheaths *in vivo* that impacts a subsequent remyelination. The recruitment of activated microglia seems to be mediated through CXCL10 upregulation in astrocytes (Fig. 13). These data corroborate the hypothesis that astrocytes are one of the key regulators in demyelinating processes of the CNS, and confirm the long-postulated crosstalk between astrocytes and microglia in demyelinating lesions. We believe that this can be extended to multiple sclerosis, where, similarly, the immune-mediated myelin damage needs to be resolved before remyelination can commence. Understanding these processes is of importance to design repair promoting therapies.

Acknowledgements

We thank I. Cierpka-Leja, S. Lang and K. Rohn for excellent technical assistance.

Funding

This work has been supported by internal funds of the Hannover Medical School (Hochschulinterne Leistungsförderung).

Supplementary material

Supplementary material is available at *Brain* online.

References

Babcock AA, Kuziel WA, Rivest S, Owens T. Chemokine expression by glial cells directs leukocytes to sites of axonal injury in the CNS. J Neurosci 2003; 23: 7922–30.

Bannerman P, Hahn A, Soulika A, Gallo V, Pleasure D. Astrogliosis in EAE spinal cord: derivation from radial glia, and relationships to oligodendroglia. Glia 2007; 55: 57–64.

Bianchi R, Kastrisianaki E, Giambanco I, Donato R. S100B protein stimulates microglia migration via RAGE-dependent up-regulation of chemokine expression and release. J Biol Chem 2011; 286: 7214–26.

Bitsch A, Schuchardt J, Bunkowski S, Kuhlmann T, Bruck W. Acute axonal injury in multiple sclerosis. Correlation with demyelination and inflammation. Brain 2000; 123: 1174–83.

Boven LA, van Meurs M, Van Zwam M, Wierenga-Wolf A, Hintzen RQ, Boot RG, et al. Myelin-laden macrophages are anti-inflammatory, consistent with foam cells in multiple sclerosis. Brain 2006; 129: 517–26.

Braun A, Dang J, Johann S, Beyer C, Kipp M. Selective regulation of growth factor expression in cultured cortical astrocytes by neuropathological toxins. Neurochem Int 2009; 55: 610–18.

Bush TG, Puvanachandra N, Horner CH, Polito A, Ostenfeld T, Svendsen CN, et al. Leukocyte infiltration, neuronal degeneration, and neurite outgrowth after ablation of scar-forming, reactive astrocytes in adult transgenic mice. Neuron 1999; 23: 297–308.

Bush TG, Savidge TC, Freeman TC, Cox HJ, Campbell EA, Mucke L, et al. Fulminant jejuno-ileitis following ablation of enteric glia in adult transgenic mice. Cell 1998; 93: 189–201.

Creed JA, DiLeonardi AM, Fox DP, Tessler AR, Raghupathi R. Concussive brain trauma in the mouse results in acute cognitive deficits and sustained impairment of axonal function. J Neurotrauma 2011; 28: 547–63.

De Keyser J, Laureys G, Demol F, Wilczak N, Mostert J, Clinckers R. Astrocytes as potential targets to suppress inflammatory demyelinating lesions in multiple sclerosis. Neurochem Int 2010; 57: 446–50.

El Hage N, Wu G, Wang J, Ambati J, Knapp PE, Reed JL, et al. HIV-1 Tat and opiate-induced changes in astrocytes promote chemotaxis of microglia through the expression of MCP-1 and alternative chemokines. Glia 2006; 53: 132–46.

Eng LF. Glial fibrillary acidic protein (GFAP): the major protein of glial intermediate filaments in differentiated astrocytes. J Neuroimmunol 1985; 8: 203–14.

Eng LF, Ghirnikar RS. GFAP and astrogliosis. Brain Pathol 1994; 4: 229–37.

Faulkner JR, Herrmann JE, Woo MJ, Tansey KE, Doan NB, Sofroniew MV. Reactive astrocytes protect tissue and preserve function after spinal cord injury. J Neurosci 2004; 24: 2143–55.

Franklin RJ, Kotter MR. The biology of CNS remyelination: the key to therapeutic advances. J Neurol 2008; 255: 19–25.

Gudi V, Moharregh-Khiabani D, Skripuletz T, Koutsoudaki PN, Kotsiari A, Skuljec J, et al. Regional differences between grey and white matter in cuprizone induced demyelination. Brain Res 2009; 1283: 127–38.

Gudi V, Skuljec J, Yildiz O, Frichert K, Skripuletz T, Moharregh-Khiabani D, et al. Spatial and temporal profiles of growth factor expression during CNS demyelination reveal the dynamics of repair priming. PLoS One 2011; 6: e22623.

Guo F, Maeda Y, Ma J, Delgado M, Sohn J, Miers L, et al. Macroglial plasticity and the origins of reactive astroglia in experimental autoimmune encephalomyelitis. J Neurosci 2011; 31: 11914–28.

Haroon F, Drogemuller K, Handel U, Brunn A, Reinhold D, Nishanth G, et al. Gp130-dependent astrocytic survival is critical for the control of autoimmune central nervous system inflammation. J Immunol 2011; 186: 6521–31.

Hesse A, Wagner M, Held J, Bruck W, Salinas-Riester G, Hao Z, et al. In toxic demyelination oligodendroglial cell death occurs early and is FAS independent. Neurobiol Dis 2010; 37: 362–9.

Katsuse O, Iseki E, Marui W, Kosaka K. Developmental stages of cortical Lewy bodies and their relation to axonal transport blockage in brains of patients with dementia with Lewy bodies. J Neurol Sci 2003; 211: 29–35.

Kieseier BC, Stuve O. A critical appraisal of treatment decisions in multiple sclerosis—old versus new. Nat Rev Neurol 2011; 7: 255–62.

Kipp M, Clarner T, Dang J, Copray S, Beyer C. The cuprizone animal model: new insights into an old story. Acta Neuropathol 2009; 118: 723–36.

Kipp M, Norkute A, Johann S, Lorenz L, Braun A, Hieble A, et al. Brain-region-specific astroglial responses in vitro after LPS exposure. J Mol Neurosci 2008; 35: 235–43.

Komoly S. Experimental demyelination caused by primary oligodendrocyte dystrophy. Regional distribution of the lesions in the nervous system of mice [corrected]. Ideggyogy Sz 2005; 58: 40–3.

Kondo Y, Adams JM, Vanier MT, Duncan ID. Macrophages counteract demyelination in a mouse model of globoid cell leukodystrophy. J Neurosci 2011; 31: 3610–24.

Koo EH, Sisodia SS, Archer DR, Martin LJ, Weidemann A, Beyreuther K, et al. Precursor of amyloid protein in Alzheimer disease undergoes fast anterograde axonal transport. Proc Natl Acad Sci USA 1990; 87: 1561–5.

Kotter MR, Li WW, Zhao C, Franklin RJ. Myelin impairs CNS remyelination by inhibiting oligodendrocyte precursor cell differentiation. J Neurosci 2006; 26: 328–32.

Lin WL, Zehr C, Lewis J, Hutton M, Yen SH, Dickson DW. Progressive white matter pathology in the spinal cord of transgenic mice expressing mutant (P301L) human tau. J Neurocytol 2005; 34: 397–410.

Lindner M, Heine S, Haastert K, Garde N, Fokuhl J, Linsmeier F, et al. Sequential myelin protein expression during remyelination reveals fast and efficient repair after central nervous system demyelination. Neuropathol Appl Neurobiol 2008; 34: 105–14.

Matsushima GK, Morell P. The neurotoxicant, cuprizone, as a model to study demyelination and remyelination in the central nervous system. Brain Pathol 2001; 11: 107–16.

Moore CS, Abdullah SL, Brown A, Arulpragasam A, Crocker SJ. How factors secreted from astrocytes impact myelin repair. J Neurosci Res 2011; 89: 13–21.

Morell P, Barrett CV, Mason JL, Toews AD, Hostettler JD, Knapp GW, et al. Gene expression in brain during cuprizone-induced demyelination and remyelination. Mol Cell Neurosci 1998; 12: 220–7.

Murphy AC, Lalor SJ, Lynch MA, Mills KH. Infiltration of Th1 and Th17 cells and activation of microglia in the CNS during the course of experimental autoimmune encephalomyelitis. Brain Behav Immun 2010; 24: 641–51.

Myer DJ, Gurkoff GG, Lee SM, Hovda DA, Sofroniew MV. Essential protective roles of reactive astrocytes in traumatic brain injury. Brain 2006; 129: 2761–72.

Nair A, Frederick TJ, Miller SD. Astrocytes in multiple sclerosis: a product of their environment. Cell Mol Life Sci 2008; 65: 2702–20.

Neumann H, Kotter MR, Franklin RJ. Debris clearance by microglia: an essential link between degeneration and regeneration. Brain 2009; 132: 288–95.

Okada Y, Yamazaki H, Sekine-Aizawa Y, Hirokawa N. The neuron-specific kinesin superfamily protein KIF1A is a unique monomeric motor for anterograde axonal transport of synaptic vesicle precursors. Cell 1995; 81: 769–80.

Paxinos G, Franklin KBJ. The mouse brain in stereotaxic coordinates. New York: Academic Press; 2001.

Qin H, Benveniste EN. ELISA methodology to quantify astrocyte production of cytokines/chemokines in vitro. Methods Mol Biol 2012; 814: 235–49.

Rasmussen S, Wang Y, Kivisakk P, Bronson RT, Meyer M, Imitola J, et al. Persistent activation of microglia is associated with neuronal dysfunction of callosal projecting pathways and multiple sclerosis-like lesions in relapsing—remitting experimental autoimmune encephalomyelitis. Brain 2007; 130: 2816–29.

Rehbinder C, Baneux P, Forbes D, van Herck H, Nicklas W, Rugaya Z, et al. FELASA recommendations for the health monitoring of mouse, rat, hamster, gerbil, guinea pig and rabbit experimental units. Report of the Federation of European Laboratory Animal Science Associations (FELASA) Working Group on Animal Health accepted by the FELASA Board of Management, November 1995. Lab Anim 1996; 30: 193–208.

Schirmer L, Merkler D, Konig FB, Bruck W, Stadelmann C. Neuroaxonal regeneration is more pronounced in early multiple sclerosis than in traumatic brain injury lesions. Brain Pathol 2012; [Epub ahead of print].

Schreiner B, Heppner FL, Becher B. Modeling multiple sclerosis in laboratory animals. Semin Immunopathol 2009; 31: 479–95.

Simard AR, Rivest S. Neuroprotective effects of resident microglia following acute brain injury. J Comp Neurol 2007; 504: 716–29.

Skripuletz T, Bussmann JH, Gudi V, Koutsoudaki PN, Pul R, Moharregh-Khiabani D, et al. Cerebellar cortical demyelination in the murine cuprizone model. Brain Pathol 2010a; 20: 301–12.

Skripuletz T, Gudi V, Hackstette D, Stangel M. De- and remyelination in the CNS white and grey matter induced by cuprizone: the old, the new, and the unexpected. Histol Histopathol 2011a; 26: 1585–97.

Skripuletz T, Lindner M, Kotsiari A, Garde N, Fokuhl J, Linsmeier F, et al. Cortical demyelination is prominent in the murine cuprizone model and is strain-dependent. Am J Pathol 2008; 172: 1053–61.

Skripuletz T, Miller E, Grote L, Gudi V, Pul R, Voss E, et al. M. Lipopolysaccharide delays demyelination and promotes oligodendrocyte precursor proliferation in the central nervous system. Brain Behav Immun 2011b; 25: 1592–606.

Skripuletz T, Miller E, Moharregh-Khiabani D, Blank A, Pul R, Gudi V, et al. Beneficial effects of minocycline on cuprizone induced cortical demyelination. Neurochem Res 2010b; 35: 1422–33.

Stadelmann C, Wegner C, Bruck W. Inflammation, demyelination, and degeneration—recent insights from MS pathology. Biochim Biophys Acta 2011; 1812: 275–82.

Tanuma N, Sakuma H, Sasaki A, Matsumoto Y. Chemokine expression by astrocytes plays a role in microglia/macrophage activation and subsequent neurodegeneration in secondary progressive multiple sclerosis. Acta Neuropathol 2006; 112: 195–204.

Voskuhl RR, Peterson RS, Song B, Ao Y, Morales LB, Tiwari-Woodruff S, et al. Reactive astrocytes form scar-like perivascular barriers to leukocytes during adaptive immune inflammation of the CNS. J Neurosci 2009; 29: 11511–22.

Voss EV, Skuljec J, Gudi V, Skripuletz T, Pul R, Trebst C, et al. Characterisation of microglia during de- and remyelination: can they create a repair promoting environment? Neurobiol Dis 2012; 45: 519–28.

Williams A, Piaton G, Lubetzki C. Astrocytes—friends or foes in multiple sclerosis? Glia 2007; 55: 1300–12.